De novo design of drug-like pMHC-targeting T-cell engagers with JAM-2

Nabla Bio

Abstract

Most therapeutic targets lie inside the cell, beyond the reach of antibodies. Peptide–MHC class I (pMHC-I) complexes display them at the surface, but a binder must distinguish its target from thousands of self-peptides on a shared MHC surface, often by a single residue. Here we show that JAM-2, our model for *de novo* biomolecular design, produces drug-quality *de novo* multispecific antibodies against pMHC-I directly from target sequence, extending zero-shot design beyond binding to multifunctionality and atomic precision. In a single, parallelized in-house campaign, JAM-2 generated binders for all five targets across two HLA alleles and three antigen classes, with routinely sub-nanomolar T-cell-activation potency, ≥216-fold selectivity against the closest human self-peptides, and clinical-grade developability. As bispecific T-cell engagers, the designs directed primary human T cells to kill peptide-presenting cells; a dual-variant anti-KRAS *de novo* design discriminated G12V and G12C from wild-type by a single side chain, killing G12V-presenting cells with EC50 = 0.07 nM. Cryo-EM confirmed this design to 0.93 Å, supporting JAM-2's atomic accuracy. These results establish *de novo* antibody design with JAM-2 as a reliable route to the intracellular proteome and pave the way for dramatically more personalized medicines.

Introduction

Only ~15% of the human cell-associated proteome is present on the cell surface[1]; the rest, including most disease-driving proteins, lies inside the cell, beyond the reach of biologics. This intracellular proteome is not entirely hidden, however. Cells converse with the immune system by continuously degrading their own proteins and presenting the fragments at the surface as peptide–MHC class I (pMHC-I) complexes, which patrolling T cells read to spare or destroy the cell[2]. A biologic that recognizes a pMHC-I complex could therefore reach these otherwise undruggable intracellular targets.

Within the complex, the MHC surface dominates and is identical across the thousands of peptides a MHC allele presents. The target peptide is short (8–11 residues) and mostly buried, exposing only a few side chains, and it can differ from an abundant self-peptide by a single residue. Failure to resolve this difference by a therapeutic can result in recognition of the self-peptide on healthy cells, making off-target toxicity a serious risk.

These constraints challenge traditional drug discovery. Isolating T-cell receptors from patient repertoires, or raising TCR-mimic antibodies by immunization and naive library screening, is slow, target-by-target, and succeeds for only a minority of pMHC targets, with clean peptide-level selectivity rarer still. Excitingly though, binders that have been successfully discovered by trial-and-error validate the target class: TCR-mimic bispecifics against p53 and mutant-RAS neoantigens show preclinical efficacy[3,4], and pMHC-targeting agents have reached the clinic, including the approved drug tebentafusp[5].

Generative biomolecular design models are improving rapidly and let the designer dictate the exact epitope and contact residues a binder engages. In principle, this control enables both the specificity that safety demands and the potency required for therapeutic impact. Less than nine months ago, we created JAM-2, a model for the fully computational design of drug-like antibodies, with strong affinities, specificities, and developability. We demonstrated it across a broad panel of soluble antigens and harder targets such as GPCRs[6]. pMHC targets are substantially harder, and progress has been partial: *de novo* miniprotein binders reach high affinity but are not antibodies and carry immunogenicity uncertainty[7,8,9], while *de novo* antibodies against pMHC have shown weak potency and little characterization of specificity or function, such as cell killing[10,11]. Computational design has not yet produced a drug-like antibody against pMHC targets.

Here we show that JAM-2 reliably designs drug-like VHH antibodies against pMHC targets. From target sequence alone, JAM-2 produced binders for 5/5 pMHCs across two HLA alleles and three antigen classes in a single parallelized campaign. Built as bispecific T-cell engagers, the designs drove T cells from human donors to kill peptide-presenting cells at sub-nanomolar potency. JAM-2 designed a dual-reactive anti-KRAS G12V and G12C antibody that shows picomolar T-cell killing as a bispecific, completely sparing wild-type, highlighting its potential as a promising therapeutic for KRAS-driven cancers. Cryo-EM confirmed that JAM-2's design for this antibody was atomically accurate, despite only using target sequences as an input. 78% of designed antibodies passed five core, industry-standard biophysical developability assays while retaining high humanness, with profiles in line with well-behaved clinical-stage molecules.

Results

JAM-2-generated *de novo* designs yield potent T-cell engagers with sub-nM T-cell activation against diverse pMHC-I targets.

We selected five pMHC-I targets across two HLA class I alleles for *de novo* design with JAM-2 (Fig. 1a). On HLA-A*02:01: the tumor-associated antigens NY-ESO-$1_{[157-165]}$ (SLLMWITQC), MAGE-$A4_{[230-239]}$ (GVYDGREHTV), and $WT1_{[126-134]}$ (RMFPNAPYL), and the oncofetal antigen $AFP_{[158-166]}$ (FMNKFIYEI). On HLA-A*03:01: the KRAS $G12V_{[7-16]}$ neoantigen (VVVGAVGVGK), arising from a codon 12 substitution present in approximately 25% of KRAS-mutant cancers[12,13] and differing from the wild-type peptide by a single residue at position 12, imposing a stringent selectivity requirement on any designed binder. These targets span three antigen classes — neoantigens, tumor associated antigens and oncofetal antigens — and two of the most prevalent HLA class I alleles in the global population.

Using only the amino acid sequences of the pMHC-I complex (comprising the peptide, HLA heavy chain, and β2-microglobulin) as input, JAM-2 generated ~84K proposed VHH designs per target, each paired with an all atom structure for the antibody-bound pMHC-I complex (Fig 1a). Peptide specificity was encoded into the design objective by specifying the solvent exposed surface of each presented peptide as the target epitope rather than the conserved MHC-I groove framework. This directed JAM-2 to prioritize contact points against the unique peptide surface over the shared MHC-I scaffold, favoring designs with no cross-reactivity against unrelated peptides presented on the same allele. Design from sequence alone renders the approach applicable to any pMHC-I target for which the peptide and HLA sequences are known. This dramatically expands access to patient-specific neoantigens, for which experimental structural characterization is rarely available.

Designs across targets were pooled into a single yeast surface display library and screened by incubation with pMHC-I tetramer (10 nM for each of the HLA-A*02:01 targets and 100 nM for KRAS G12V) assembled from each cognate peptide–HLA pair, as well as off-target tetramers to assess cross-reactivity. Tetramer-positive populations were isolated by two rounds of FACS and enriched sequences were identified by next-generation sequencing (Fig. 1a, Suppl. Fig. 1). Successful designs were recovered across all five targets, with per-target hit rates ranging from 0.06% (KRAS G12V; 48 binders) to 3.10% (AFP; 2,558 binders), and intermediate rates of 1.27%, 1.16%, and 0.27% for NY-ESO-1 (1,075 binders), WT1 (973), and MAGE-A4 (232), respectively (Fig. 1b). Binding was highly target-restricted: designs enriched against each target yielded no more than 16 off-target binders against any other pMHC-I tetramer, compared with 48–2,558 on-target binders, with the highest off-target signal observed toward the AFP complex (Fig. 1b).

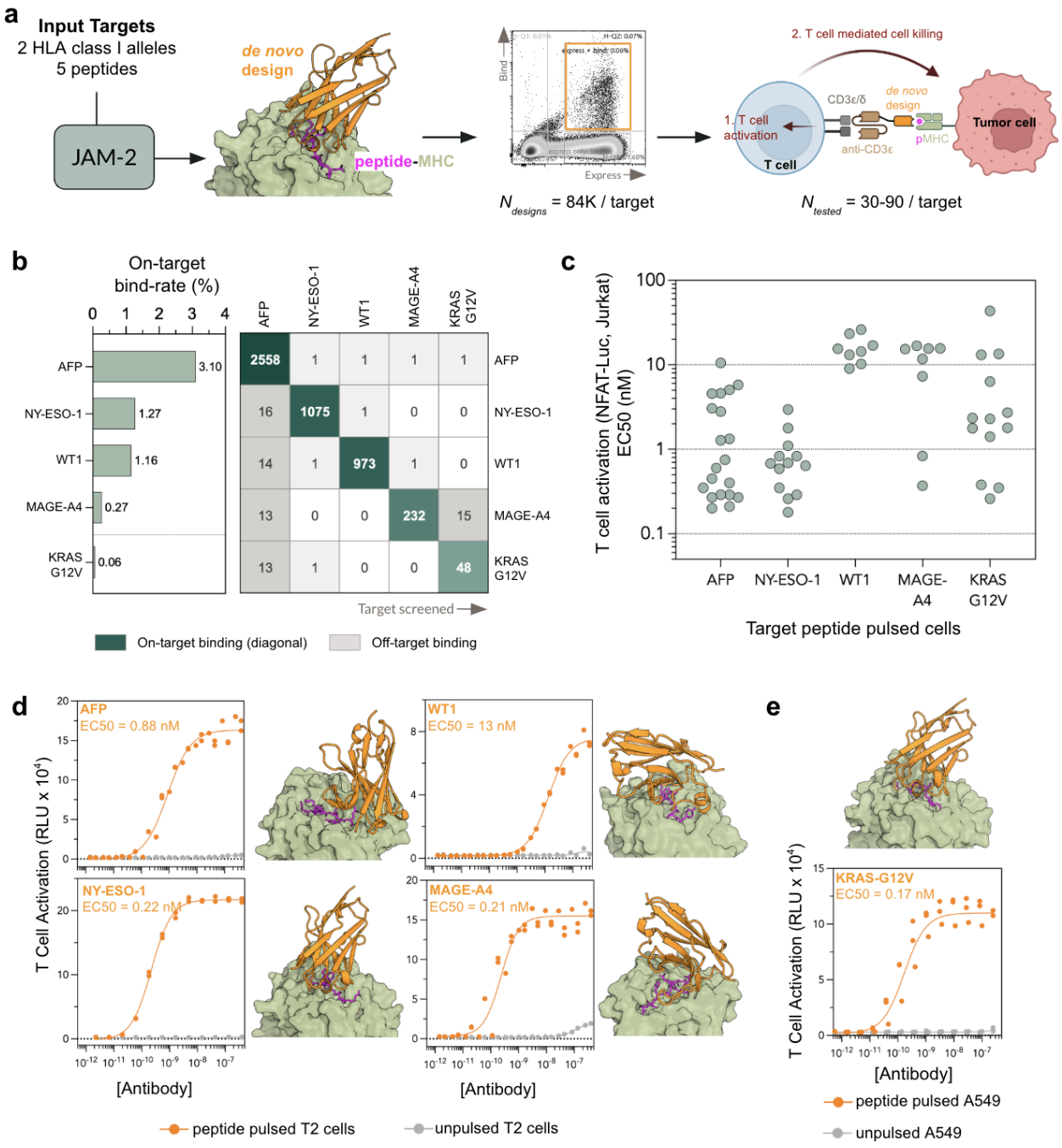

Figure 1. JAM-2-generated *de novo* designs yield potent T cell engagers with sub-nM T cell activation against diverse pMHC-I targets. (a) Design and screening workflow. JAM-2 *de novo* designed VHH antibodies against five pMHC-I complexes spanning two HLA class I alleles. 84,000 *de novo* designs per target were displayed on yeast and screened against cognate and off-target pMHC-I tetramers by FACS. Enriched binders (30-90/target) were reformatted as VHH–anti-CD3ε scFv bispecific T-cell engagers (TCEs), and evaluated for T-cell activation and, for a subset, T-cell-mediated tumor cell killing. **(b)** Left: on-target bind rate (% designs binding the cognate tetramer) per target by YSD. Right: cross-reactivity matrix showing the number of confirmed tetramer-positive binders for designs from each campaign (rows) screened against each target (columns). On-target (diagonal) values in teal; off-target in grey. KRAS G12V was screened at 100 nM tetramer, all others at 10 nM. **(c)** T-cell activation EC50 (NFAT-luciferase Jurkat reporter) for lead TCEs against peptide-pulsed cells across all five targets. **(d, e)** T-cell activation

dose–response curves for lead TCEs against peptide-pulsed (orange) versus unpulsed (grey) cells, each with EC50 values and representative JAM-2-predicted VHH:pMHC-I structural models. Data were collected in at least duplicate. **(d)** The four HLA-A*02:01 targets (AFP, NY-ESO-1, WT1, MAGE-A4) on T2 cells. (e) KRAS G12V on HLA-A*03:01^{+} A549 cells.

Up to 90 YSD-enriched designs per target were reformatted as VHH–scFv bispecific T-cell engagers (TCEs), pairing each *de novo* designed pMHC-I-targeting VHH with an anti-CD3ε scFv, derived from clinical-stage Duvortuxizumab[14] (Fig. 1a). TCE activity was evaluated using a Jurkat-NFAT luciferase reporter assay (BPS Bioscience) with HLA-A*02:01^{+} T2 cells (NY-ESO-1, MAGE-A4, AFP, and WT1 targets) or HLA-A*03:01^{+} A549 cells (KRAS G12V) pulsed with cognate peptides (Fig. 1c-e). All designs were evaluated at a single concentration of 10 nM antibody (Suppl. Fig. 2a-b), and then up to 24 top performing designs per target were titrated to evaluate full dose-response curves (Fig. 1c-e).

TCE evaluation revealed potent, peptide-dependent T-cell activation across all five targets, with negligible background activity against unpulsed cells (Suppl. Fig. 2c-d). Remarkably, top-performing designs for four out of the five targets exhibited sub-nanomolar potencies, led by KRAS G12V (EC50 = 0.17 nM), MAGE-A4 (EC50 = 0.21 nM), NY-ESO-1 (EC50 = 0.22 nM), and AFP (EC50 = 0.88 nM) (Fig. 1d,e). The WT1 target also showed robust T-cell activation, with the top-performing design achieving a double-digit nanomolar EC50 = 13 nM (Fig. 1d).

Representative JAM-2-predicted VHH:pMHC-I structural models are shown alongside the dose-response data (Fig. 1d,e); in each model, the designed VHH is positioned precisely over the solvent-exposed peptide rather than the conserved MHC-I framework, confirming that the observed peptide-dependent activation is driven by the intended structure-based design objective.

De novo VHH-TCEs recognize NY-ESO-1 with single-residue precision with no human self-peptide cross-reactivity

For therapeutic application, pMHC-I-targeting antibodies must discriminate the target peptide from the self-peptide repertoire of the presenting HLA allele. We assessed the peptide specificity across designs against two target peptides and alleles: NY-ESO-1/HLA-A*02:01 and then the single-residue mutant KRAS G12V/HLA-A*03:01.

For *de novo* designed anti-NY-ESO-1 VHH TCEs, we measured T-cell activation against two on-target peptides — the native 9C (SLLMWITQC) and the anchor-modified 9V analog (SLLMWITQV). The 9V analog is widely utilized in NY-ESO-1 immunotherapies because its C-terminal cysteine-to-valine substitution improves HLA-A*02:01 binding affinity and complex stability[17]. Without any experimental affinity maturation or optimization, lead *de novo* designs immediately reached the activation regime of two affinity-matured positive controls — NYA-0060 (Mie University/Daiichi Sankyo[15]) and the structure-evolved T3 Fab (Stewart-Jones et al.[16]) (Fig. 2a). In full dose-response titrations, these unoptimized designs acted as potent on-target activators, eliciting EC50 values as low as 0.22 nM against the 9V peptide (Fig. 2b).

To challenge the selectivity of our *de novo* designs, we utilized a panel of five HLA-A*02:01 off-target peptides drawn from the in silico screen of 14,363 9-mer HLA-A*02:01 peptides

reported by Householder et al.[9] These five sequences represent the HLA-A*02:01 self-peptides whose residues most closely resemble the NY-ESO-1 epitope, making them the off-target antigens most likely to drive severe, off-tumor toxicities *in vivo*.

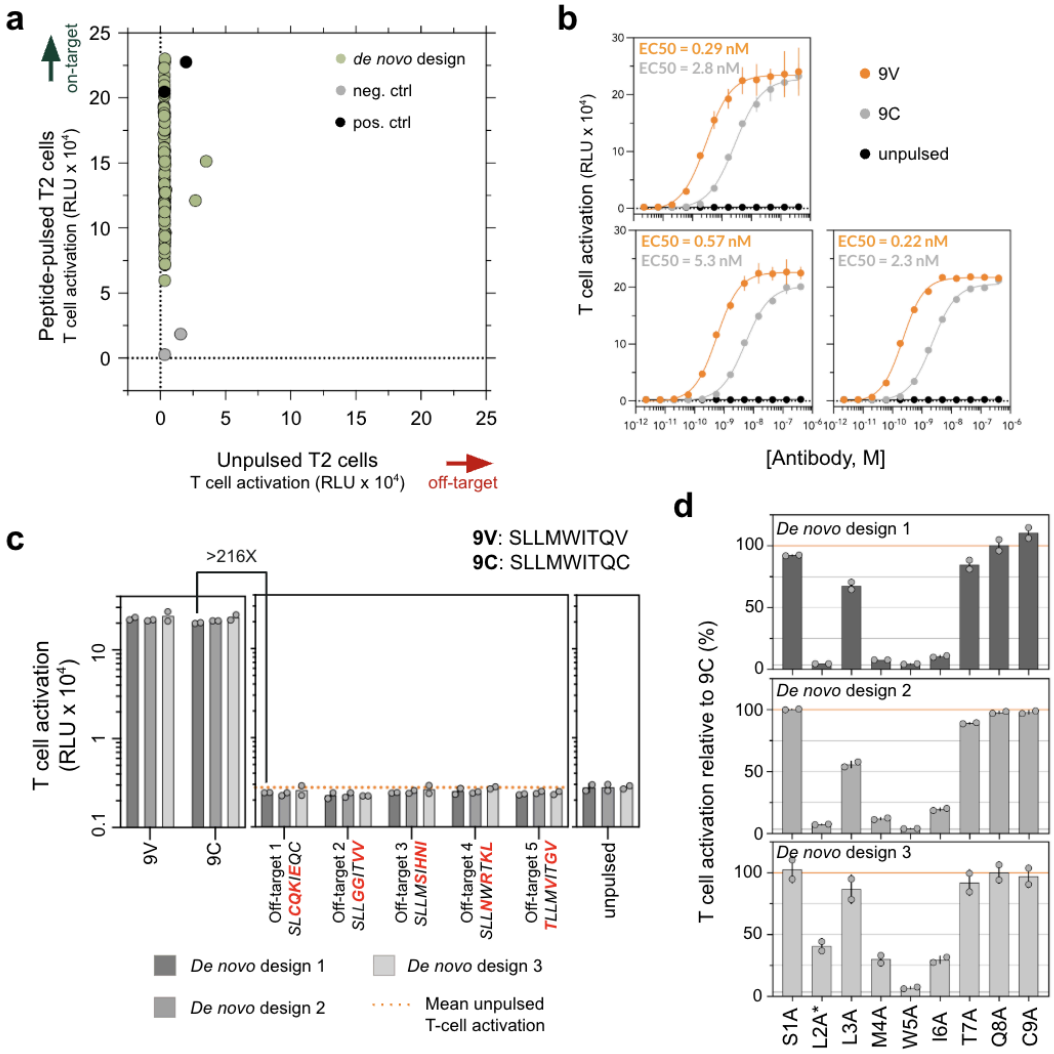

Figure 2. JAM-2 *de novo* designs selectively target NY-ESO-1 over its closest self-peptides, with no off-target activation (a) T-cell activation (NFAT-luciferase Jurkat reporter; RLU x10⁴) by *de novo* VHH-TCE designs against NY-ESO-1 9V (SLLMWITQV)-pulsed (y-axis) versus unpulsed (x-axis) HLA-A*02:01⁺ T2 cells. *De novo* designs (green), isotype negative control (grey), and positive controls (black; NYA-0060, Daiichi Sankyo[15]; T3, Stewart-Jones et al.[16]); dotted lines mark baselines. Designs near the y-axis combine high on-target with low off-target activation. **(b)** Dose-response curves and EC50 values for three lead designs against 9V (orange), 9C (SLLMWITQC, grey), and unpulsed (black) T2 cells. **(c)** T-cell activation for the three leads against 9V, 9C, five HLA-A*02:01 off-target peptides (residues differing from the NY-ESO-1 epitope in red), and unpulsed cells; dotted orange line, mean unpulsed activation; bracket marks ≥216-fold selectivity of 9C over the off-targets. Off-targets are the most sequence-similar to the NY-ESO-1 peptide from an in silico screen of 14,363 HLA-A*02:01 9-mers (Householder et al.[9]). **(d)** Alanine scan of the 9C peptide for the three leads; each bar is a single alanine substitution at the indicated position, plotted as % T-cell activation relative to unmodified 9C (orange line). Asterisk denotes positions with substantial predicted loss of HLA-A*02:01 binding relative to 9C (>4-fold IC_{50}; Suppl. Table 1). Panels (a, c, d) used 400 nM TCE; all data are mean ± SD of at least duplicate measurements.

Across three lead *de novo* designs, all five off-target peptides drove T-cell activation at or below the background levels observed in unpulsed cells (Fig. 2c; Suppl. Fig. 3). Each tested *de novo* design discriminated the on-target peptide from the closely related off-target peptides by at least 216-fold in an NFAT-luciferase reporter assay. Since the off-target-induced reporter activity was statistically indistinguishable from the unpulsed controls and fell below the assay's limit of detection, this fold-change represents a conservative lower bound on functional selectivity dictated by the assay's dynamic range, rather than a maximum measured ceiling.

To map the exact molecular contacts driving this specificity, we performed an alanine scan of the 9C peptide (SLLMWITQC), measuring functional NFAT activation relative to the unmodified 9C wild-type sequence (Fig. 2d). Across all three tested designs, alanine substitutions at the central, solvent-exposed residues – Met4 and Trp5 – severely abrogated T-cell activation. Substitution at position Trp5 exerted the most profound effect, crashing activation to 8% of the wild-type 9C signal and identifying this as a principal contact point for the *de novo* designs. Ile6 substitution similarly impaired activation despite low solvent exposure, suggesting it plays a role in maintaining optimal geometry of the proximal Met4 and Trp5 residues. Conversely, peripheral substitutions at Ser1, Thr7, Gln8, and the C-terminal anchor Cys9 were well tolerated (≥85% activation)[18]. This pattern indicates that physical recognition by the *de novo* designs is precisely directed toward the unique, solvent-exposed peptide surface rather than the conserved MHC-I framework. The reduced activation observed upon Leu2 substitution most likely reflects the disruption of the dominant HLA-A*02:01 P2 anchor residue, which decreases overall peptide presentation density on the cell surface, rather than a loss of direct contact by the design (Suppl. Table 1).

De novo designed VHH-TCEs show single-residue programmable selectivity across oncogenic KRAS variants while sparing wild-type

Oncogenic KRAS codon-12 mutations differ from the wild-type protein by a single amino acid. In the HLA-A*03:01-restricted decapeptide epitope VVVGAXGVGK (KRAS residues 7–16), the position-12 residue (X) is substituted with valine (G12V), cysteine (G12C), or aspartate (G12D), contrasting with the native glycine present in the wild-type sequence. Critically, therapeutic antibodies targeting this epitope must stringently discriminate any oncogenic peptide from the wild-type sequence to prevent severe off-tumor toxicities.

Across all 14 activating KRAS G12V VHH-TCE designs, no T-cell activation was observed against wild-type–pulsed A549 cells above the baseline of unpulsed cells, establishing single-residue G12V-versus-wild-type discrimination as a consistent property of the JAM-2 designs (Fig. 3a, Suppl. Fig. 4). From a single round of *de novo* design, without optimization, the highest-magnitude design reached a 32-fold G12V activation window over wild-type, significantly exceeding the 8-fold window of the in-plate positive control—a phage display–derived anti–KRAS G12V/HLA-A*03:01 antibody developed by Biocytogen[19].

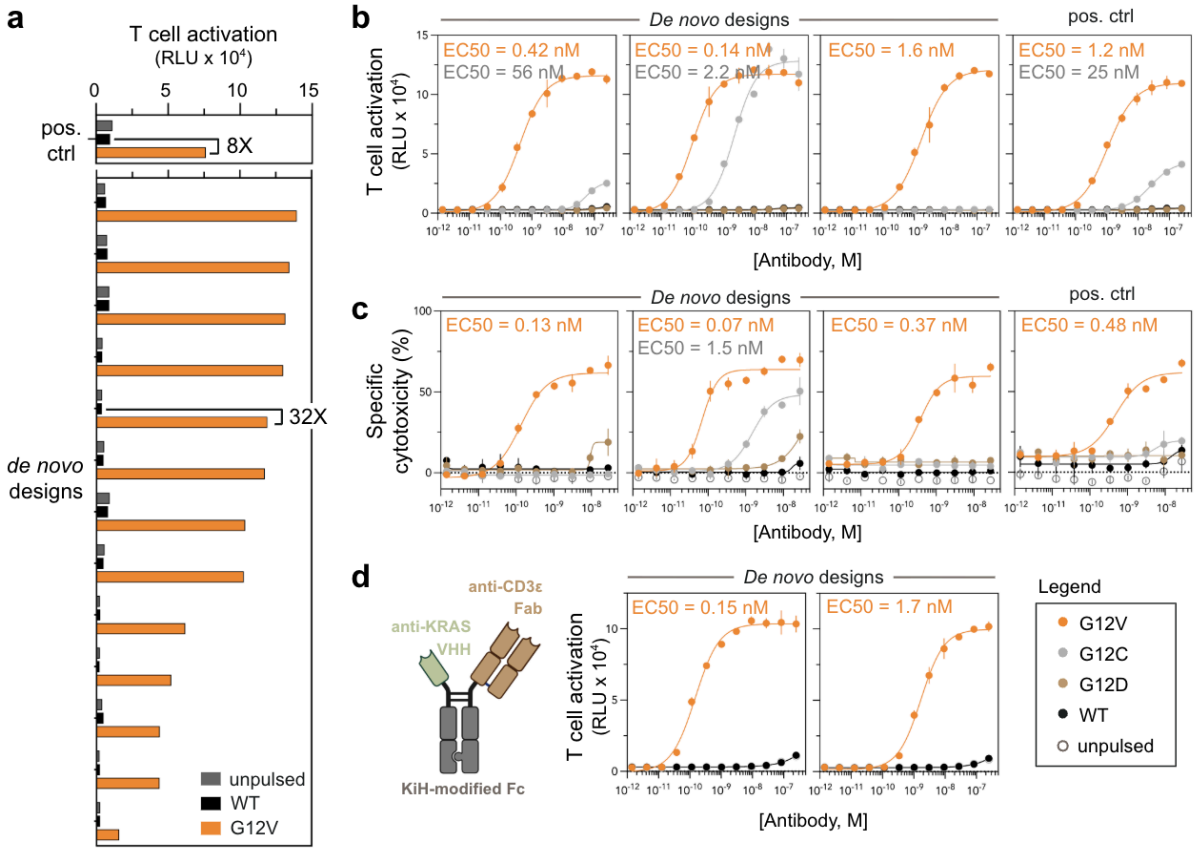

Figure 3. Anti-KRAS *de novo* designs achieve potent, single-residue-selective T-cell activation and cytotoxicity. (a) Single-concentration screen (250 nM TCE) of 14 *de novo* VHH-TCE designs by T-cell activation (Jurkat-NFAT reporter) against HLA-A*03:01⁺ A549 cells pulsed with KRAS G12V peptide (VVVGAVGVGK; orange), wild-type peptide (black), or left unpulsed (grey). Bars are ranked by G12V activation; brackets give fold G12V-over-WT activation for the most selective design (32-fold) and the positive control (a KRAS G12V-targeting antibody from Biocytogen[19]; 8-fold). **(b)** Dose-response T-cell activation and **(c)** PBMC specific cytotoxicity for three lead designs and the positive control against the same A549 targets pulsed with KRAS G12V, G12C, G12D, or wild-type peptide; **(c)** also includes unpulsed cells. Specific cytotoxicity = (1 − (%live_TCE / %live_no-TCE)) × 100; effector:target 10:1, 48 h co-culture. **(d)** Left: bispecific schematic of the *de novo* anti-KRAS G12V VHH and an anti-CD3ε Fab (Duvortuxizumab[14]) on a knobs-into-holes (KiH) heterodimeric Fc. Right: dose-response T-cell activation for two leads reformatted from VHH-scFv into this full-length bispecific, against G12V- or wild-type-pulsed A549 cells. Data are mean ± SD of at least duplicate measurements. G12V, orange; wild-type, black; unpulsed, open grey circles; G12C, grey and G12D, tan in (b, c) only. EC50 values shown for G12V and, where measurable, G12C.

A single therapeutic agent that engages multiple pathogenic KRAS variants would broaden the treatable patient population, increasing impact for the same development cost. Conventional discovery campaigns, however, typically optimize for a single target variant, relying on stochastic cross-reactivity to engage related mutants. JAM-2-based *de novo* design is not constrained in this way: here, we specified the design objective residue by residue, requiring strict selectivity against wild-type glycine while deliberately maintaining latitude for chemically similar hydrophobic or polar substitutions at the G12V position.

We tested whether JAM-2 VHH-TCEs designed against G12V cross-react with related codon-12 variants. T-cell activation assays against peptide-pulsed A549 cells showed the lead designs spanned a predictable spectrum of functional phenotypes (Fig 3b). In particular, one design acted as a potent dual-variant engager, robustly activating T cells against both G12V and G12C (EC50s = 0.14 nM and 2.2 nM). No activation above background was observed against wild-type or G12D targets for any design (Fig. 3b). Furthermore, the top-performing JAM-2 *de novo* designs matched or exceeded the benchmark positive control's activation potency (G12V EC50 as low as 0.14 nM vs 1.2 nM for the benchmark antibody). Binding affinity for the dual-variant anti–KRAS G12V VHH was additionally confirmed by flow cytometry and BLI (Suppl. Fig. 5).

These designs also translated into highly potent cytotoxic effectors. In peripheral blood mononuclear cell (PBMC) killing assays against peptide-pulsed A549 cells — providing a translationally relevant readout of primary human T cell-mediated lysis — all three leads drove sub-nanomolar killing of G12V targets (EC50 = 0.07–0.37 nM) (Fig. 3c). Mirroring the activation profiles, the dual-variant lead design successfully eliminated G12C-pulsed cells (EC50 = 1.5 nM), while no design mediated lysis of wild-type- or G12D-pulsed targets above background levels. The most potent design outperformed the Biocytogen benchmark (EC50 = 0.07 nM vs 0.48 nM). These results demonstrate that a single, unoptimized JAM-2-designed VHH-TCE can effectively address both KRAS G12V and G12C variants, which together account for ~35% of all KRAS-mutant malignancies[12].

All functional data above was generated in a tandem VHH-anti-CD3ε scFv (VHH-TCE) format, which shares the liabilities of the Fc-less tandem-scFv/BiTE class[20,21]. To test whether the designs tolerate a more clinically tractable scaffold, we reformatted lead anti-KRAS designs as knobs-into-holes (KiH) IgG-like bispecifics[22]. Two of three leads were confirmed as correctly assembled heterodimers by analytical SEC (Suppl. Fig. 6), and each retained peptide-dependent NFAT activation against target cells, demonstrating that the potency and specificity of the *de novo* designs successfully transfer across distinct formats (Fig. 3d).

A cryo-EM structure confirms the designed binding mode and the structural basis of G12V selectivity

To test whether the binding mode JAM-2 predicted for the lead anti–KRAS G12V VHH matched the molecule's actual structure, we determined a cryo-EM reconstruction of the VHH bound to the KRAS G12V (VVVGAVGVGK) peptide presented by HLA-A*03:01, with an anti-β2m Fab included as a fiducial. From 566,000 particles the map reached 3.30 Å nominal resolution (FSC = 0.143), improving to 3.25 Å across the VHH–pMHC interface after local refinement (Fig. 4a,b; Suppl. Fig. 7-8, Suppl. Table 2). The density placed the VHH directly over the peptide-binding groove, engaging the solvent-exposed face of the peptide (Fig. 4a).

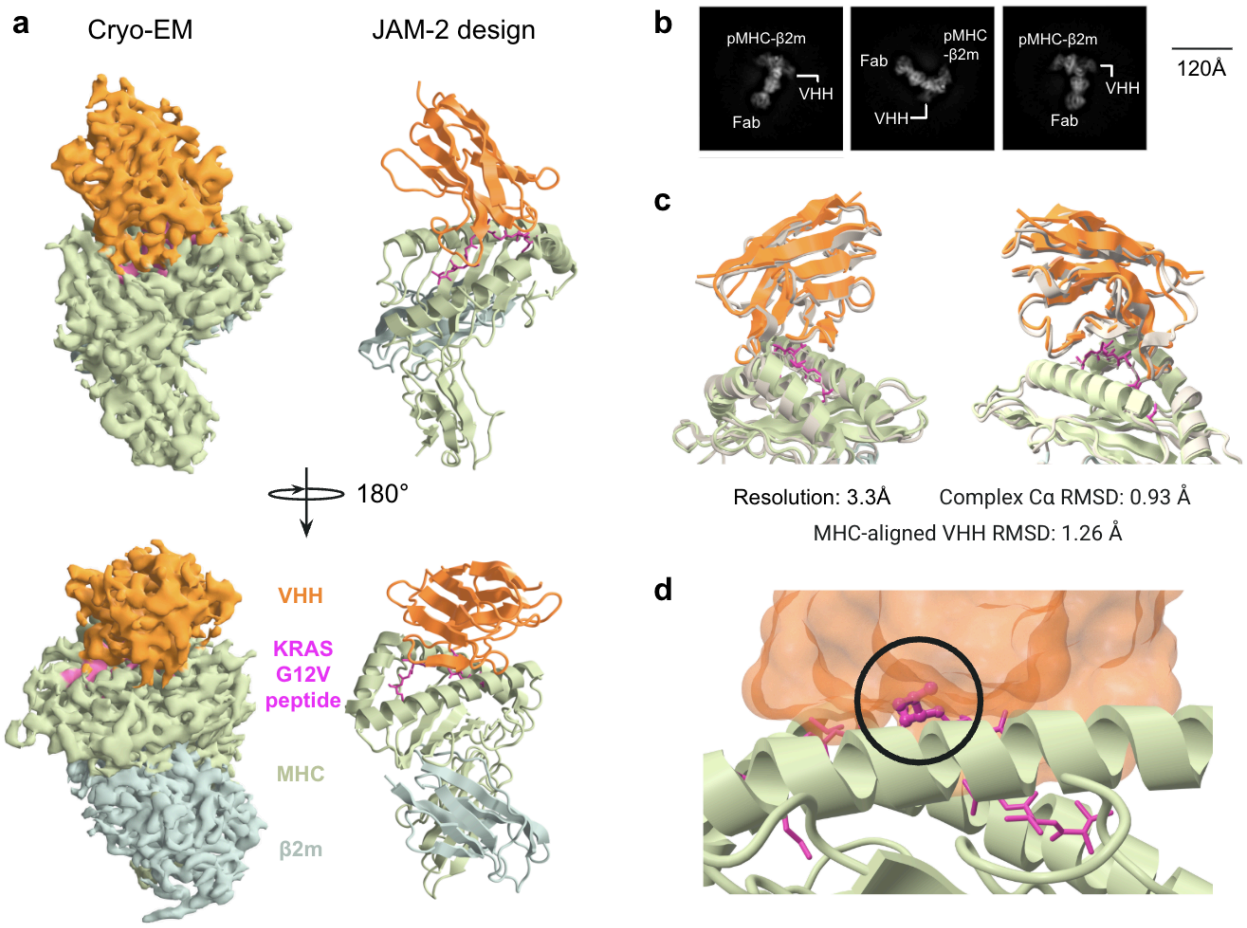

Figure 4. Cryo-EM confirms the JAM-2-designed anti–KRAS G12V VHH:pMHC complex at atomic accuracy and reveals the basis of variant recognition. (a) Cryo-EM density (left) and JAM-2 design model (right) of the VHH bound to KRAS G12V:HLA-A*03:01:β2m, in two orientations 180° apart. VHH, orange; KRAS G12V peptide, magenta; MHC, light green; β2m, light blue. (b) Two-dimensional class averages (anti-β2m Fab fiducial); pMHC-β2m, Fab, and VHH densities are well resolved. Scale bar, 120 Å. (c) Design (colored) superposed on the experimental structure (grey): whole-complex Cα RMSD 0.93 Å, and 1.26 Å for the VHH after alignment on the MHC. Global resolution 3.3 Å (3.25 Å at the interface). (d) Interface close-up (VHH surface, peptide sticks): the Val12 side chain (circled), the only difference from wild-type Gly12, inserts into a complementary VHH pocket, the basis for variant-selective recognition.

The experimental structure closely matched the model generated during design. A least-squares superposition of the designed complex onto the refined coordinates gave a Cα RMSD of 0.93 Å over the entire VHH–pMHC complex (0.998 Å over all 2,024 backbone atoms of 506 residues; Fig. 4c). The agreement extended to the docking geometry, not merely the folds: with the structures aligned on the MHC alone (0.84 Å RMSD), the VHH still superimposed to 1.26 Å Cα RMSD, indicating that the design reproduced the approach angle and register of the antibody on the pMHC (Fig. 4c).

In keeping with the design objective, which steered the paratope toward the solvent-exposed peptide rather than the conserved MHC groove, the interface was strongly peptide-focused. The VHH buried 1,018 Å² of the pMHC surface; although the much larger MHC platform accounted for most of this (687 Å², 68%), the 10-residue peptide contributed 331 Å² (32%), and 29% of the VHH's heavy-atom contacts were made to the peptide. On a per-residue basis these contacts

peaked sharply at the mutated position rather than being distributed along the peptide, consistent with the peptide-directed specificity seen functionally.

The structure also rationalizes the single-residue G12V-over-wild-type discrimination (Fig. 4d). The Val12 side chain — the sole chemical difference from wild-type KRAS, which carries Gly at this position — inserted into a complementary hydrophobic pocket on the VHH and was essentially fully buried (side-chain solvent-accessible surface 109.9 → 0 Å² on complex formation). Discrimination was packing-driven rather than hydrogen-bond-driven: the single VHH–peptide backbone hydrogen bond at position 12 is also available in wild-type KRAS, so selectivity derives from filling the pocket, not from a new polar contact. Because recognition keys on packing the position-12 side chain into this pocket rather than on a fixed polar contact, it depends on that residue's size and chemistry: the side-chainless wild-type Gly cannot engage the pocket and the charged Asp of G12D is disfavored, whereas small, nonpolar substitutions can be accommodated. This packing-based readout offers a structural rationale for the programmable variant selectivity seen functionally (Fig. 3) — designs could be tuned to recognize G12V alone, or both G12V and G12C, while sparing wild-type and G12D — and for the complete loss of activation against wild-type KRAS across all 14 functional G12V designs and the 32-fold G12V-over-WT window of the lead.

JAM-2 anti-pMHC *de novo* designs exhibit drug-like biophysical properties

A key advantage of JAM-2-based *de novo* design is the potential to encode developability into the design objective, bypassing post-hoc optimization[6]. Developability — the biophysical properties governing an antibody's manufacturability, stability, and specificity — is a central gatekeeper in biologics development, predictive of both preclinical liabilities and clinical success[24]. To test the *de novo* designed antibody independently of the bispecific format, we assessed the biophysical properties of up to 8 designs in VHH-Fc format per target expressed in ExpiCHO and then purified, profiling expression titer, monomericity, thermal stability, and polyreactivity. Overall, 78% of designs passed all biophysical developability criteria across five assays (Fig. 5a), with per-target pass/fail profiles shown per design in Fig. 5b. Expression titers exceeded the 150 mg/L threshold for 38/38 (100%) designs (Fig. 5c). Differential scanning fluorimetry (DSF) showed clear melting profiles, yielded melting temperatures of 60–72°C, with 34/36 (94%) of designs passing the 65°C threshold (Fig. 5d). Size-exclusion chromatography (SEC) confirmed >90% monomeric elution profiles for 31/37 (84%) of designs (Fig. 5e); the principal exception was a subset of NY-ESO-1 designs that fell below the 90% monomericity cut-off. Across polyreactivity assays, a majority of designs showed less polyreactivity than even trastuzumab, with 35/38 (92%) and 38/38 (100%) of designs showing scores at or below the 50%-bococizumab threshold in PAIA-OVA and BVP ELISA respectively (Fig. 5f,g). As an additional, sequence-based metric, humanness, a proxy associated with reduced immunogenicity risk, was measured as the percent identity of each *de novo* designed VHH domain to its nearest human germline V gene. Humanness exceeded 80% for 33/39 (85%) of *de novo* designs (Fig. 5h). Together, these metrics demonstrate that JAM-2 generates developable, drug-like anti-pMHC binders straight out of the model, bypassing the need for downstream engineering.

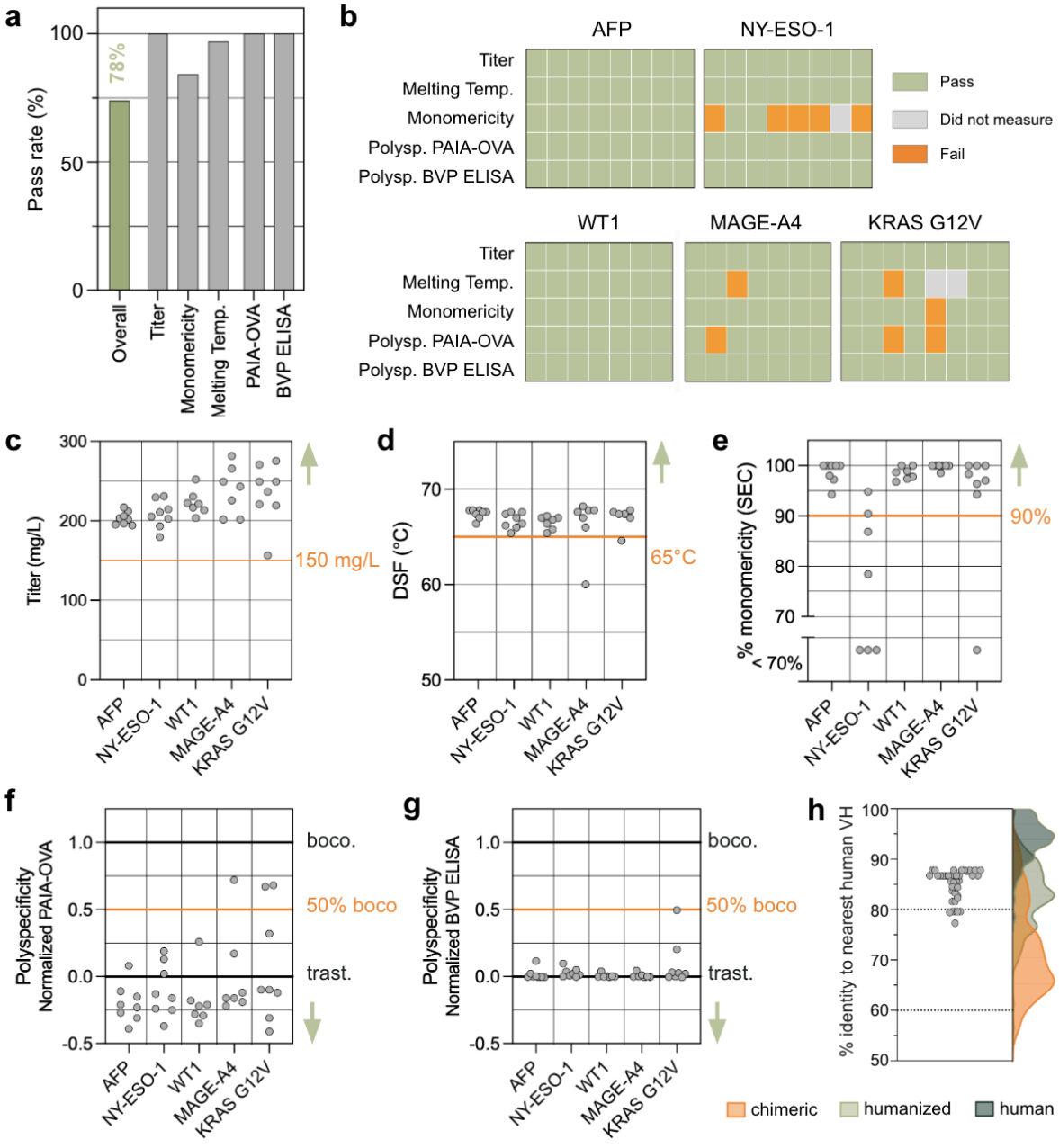

Figure 5: JAM-2-generated anti-pMHC *de novo* designs show clinical-grade developability. (a) Overall pass rate across all designs (green, 78%) and per-assay pass rates (grey) **(b)** Per-target pass/fail matrix by metric (titer, melting temperature, monomericity, polyspecificity by PAIA-OVA and BVP ELISA). Green, pass; grey, not measured; orange, fail. **(c–g)** Assay-value distributions across targets; each point is one *de novo* design, orange lines mark reference antibodies or thresholds, and the green arrow shows the desirable direction. Missing points indicate insufficient material or an assay not performed. **(c)** Expression titer (mg/L); threshold 150 mg/L. **(d)** Thermal stability by differential scanning fluorimetry (DSF), melting temperature (°C); threshold 65 °C. **(e)** Monomericity by size-exclusion chromatography (SEC, %); threshold 90%. **(f, g)** Polyreactivity by **(f)** PAIA-OVA and **(g)** BVP ELISA, normalized between low-reactivity trastuzumab ("trast.", 0) and high-reactivity bococizumab ("boco.", 1.0); threshold 50% of bococizumab. **(h)** Sequence humanness, percent identity of the VHH domain to its nearest human VH germline (points), against reference distributions for chimeric (orange), humanized (light green), and human (dark green) antibodies.

Discussion

Our results show that JAM-2 reliably *de novo* designs drug-like VHH antibodies against pMHC targets directly from target sequence, without immunization, naive library screening, or iterative optimization. In a single campaign across five targets spanning two HLA alleles and three antigen classes, it produced binders for 5/5 targets with most designs meeting all early stage developability criteria without optimization. Reformatted as bispecific T-cell engagers without any further optimization, these drove primary human T cells to kill peptide-presenting cells at sub-nanomolar potency. To our knowledge, this is the first fully computationally designed antibody shown to drive potent, antigen-specific T-cell killing through pMHC, the property that defines a therapeutic candidate against this class. Lead designs retained potency and specificity when moved from the tandem VHH-scFv into an IgG-like knobs-into-holes bispecific, showing the target recognition is not tied to a single format.

For pMHC, the central challenge is specificity, not affinity: a binder must identify its target peptide among thousands of near-identical self-peptides on a shared MHC surface, often differing by only a single residue, or risk attacking healthy cells. JAM-2 met this bar by design. This is most clearly highlighted in a single anti-KRAS design that engages the G12V and G12C oncogenic peptides while sparing wild-type, a distinction turning on one side chain, and kills at 0.07 nM. Cryo-EM of a lead complex matched the design at atomic accuracy, confirming that the model places its contacts where intended — the structural basis for the single-residue discrimination. These *in vitro* results lay the groundwork for the next test: resolving proteome-wide off-target liabilities, beyond the nearest self-peptides examined here, *in vivo* — where tumor control and tolerability can be verified directly.

Targeting pMHC also extends antibodies to otherwise undruggable biology. Most disease drivers act inside the cell, and their MHC-presented peptides are the only externally visible trace of them, so designing against these complexes opens intracellular targets — transcription factors, fusion oncoproteins, mutated drivers — to antibodies. Since designs come directly from amino acid sequence and do not require structural information, discovery is fast and readily parallelized. This may matter most for neoantigens, defined by a patient's own mutation and HLA type, where a sequence-driven method could in principle reach a candidate on a timescale that screening cannot. Together, these results establish *de novo* design as a route to the intracellular proteome, shifting the rate-limiting step from antibody discovery to target selection.

Finally, these advances extend medicine's long arc from blunt to precise. Chemotherapy and radiation strike every dividing cell; decades ago, targeted agents like imatinib and trastuzumab narrowed treatment to a single oncoprotein; today, genotype-matched drugs and engineered T cells tune it to a tumor's molecular profile. Each step sharpens the line between diseased and healthy cells, widening the margin between treating disease and harming the patient. JAM-2 carries this trajectory to atomic resolution: using nothing more than sequence, a binder can now be rapidly designed, built, and validated to read a single side chain — and, for a neoantigen, one unique to a single patient. This not only improves accessibility to the intracellular proteome, but also paves a new path for dramatically more personalized therapies.

Experimental Methods

De novo designed yeast surface display library construction

To construct the yeast surface display libraries, oligonucleotides encoding the designed VHH antibodies were ordered from Twist Biosciences as 300-nt oligo pools with flanking BsaI recognition sites for Golden Gate assembly. All DNA was codon-optimized for expression in *S. cerevisiae*. Golden Gate assembly reactions were run overnight using PCR-amplified oligo pool DNA to clone into the yeast display vector, pCTcon2.

Purified Golden Gate reactions were electroporated into NEB 10-beta electrocompetent *E. coli* (New England Biolabs) using the pre-set bacterial protocol on the Gene Pulser Xcell electroporation system (BioRad). Serial dilutions of the bacterial transformants were plated and verified to represent a greater than 100-fold coverage of the library. The transformed cells were cultured overnight, shaking at 37°C in LB media (Teknova) under carbenicillin selection. The resulting plasmid library was extracted from the bacterial cultures using a QIAprep Spin Miniprep kit (QIAGEN).

The assembled libraries were linearized and transformed into *S. cerevisiae* strain EBY100 (ATCC) using a standard lithium acetate and DTT-based yeast electroporation protocol as described by Van Deventer et al.[25] Transformants were serially diluted and plated post recovery to verify library coverage was at least 100-fold. Yeast transformants were cultivated in synthetic dextrose medium with casamino acids (SDCAA) pH 4.5 (Teknova) shaking at 30°C overnight.

Fluorescence-activated cell sorting of yeast surface displayed antibody libraries

Yeast libraries were grown to saturation overnight in SDCAA pH 4.5 media shaking at 30°C. Each library was passaged into fresh SDCAA pH 4.5 media at a 25X dilution and grown for 2-4 hours before pelleting via centrifugation at 2000 x g for 5 minutes. To induce the libraries, cell pellets were resuspended to an OD600 of 1 in synthetic galactose medium with casamino acids (SGCAA) (Teknova) and incubated at 20°C for 20 hours.

For sorting, induced yeast cells were washed twice with 1% PBSA (1% BSA in 1x PBS). The libraries were incubated with anti-c-Myc-AF488 antibody (1:100 dilution, 16-308, Sigma-Aldrich) to label yeast cells displaying full length VHHs, and the desired antigen concentrations to evaluate antigen binding for 1 hour at room temperature. The pMHC antigens and concentrations are summarized in Table 1. The samples were spun down at 4°C and washed twice with ice-cold 1% PBSA to remove unbound antigen and c-Myc antibody. Each sample was then stained with anti-His-AF647 secondary antibody (1:100 dilution, IC0501R, R&D Systems), and the samples were incubated on ice for 30 minutes. The samples were spun down at 4°C and washed twice with ice-cold 1% PBSA to remove any excess secondary antibody.

Samples were sorted on a Sony SH800 cell sorter using normal or ultra purity mode depending on the stage of enrichment. Sorted binders were collected in SDCAA pH 4.5 media and shaken at 30°C for 2-3 days until saturated.

Table 1. Peptide-MHC reagent and yeast surface display library enrichment information.

HLA Allele	Peptide Target	pMHC antigen format	Product Information	First Enrichment	Second Enrichment
HLA-A*02:01	AFP [158-166] FMNKFIYEI	tetramer	Kactus Bio MHC-HM407T	10 nM	10 nM
	MAGE-A4 [230-239] GVYDGREHTV	tetramer	Kactus Bio MHC-HM401T	10 nM	10 nM
	NY-ESO-1 [157-165] SLLMWITQC	tetramer	Acro Biosystems HL1-H52E8	10 nM	10 nM
	WT1 [126-134] RMFPNAPYL	tetramer	Acro Biosystems HLW-H52E6	10 nM	10 nM
HLA-A*03:01	KRAS [7-16] G12V VVVGAVGVGK	tetramer	Kactus Bio MHC-HM418T	100 nM	100 nM

Next generation sequencing of sorted yeast surface display populations

Binders isolated from the second enrichment were yeast miniprepped using a Zymoprep Yeast Plasmid Miniprep II kit (Zymo Research). DNA was then electroporated into NEB 10-beta electrocompetent *E. coli* (New England Biolabs) and recovered in LB media supplemented with carbenicillin. *E. coli* cultures were miniprepped using a QIAprep Spin Miniprep kit (QIAGEN) and then submitted for sequencing using Oxford Nanopore technology. Nanopore reads were mapped to the coding DNA of JAM-2-generated VHHs, and the number of reads that aligned to each design was tabulated. Due to sequencing noise, some designs had non-zero but low read count levels, whereas designs truly present in the binding population have higher read counts. To classify binders from non-binders, we set a read count threshold based on the empirical cumulative distribution function (ECDF) of read counts in the sample. Typically, 80-90% of reads are accounted for by a small number of designs, and the presence of clear “elbow” in the ECDF suggests a natural read count threshold that separates non-binders from binders. Empirically, we have validated this strategy identifies binding designs such that when expressed recombinantly and tested individually, designs are highly likely to bind the target.

Protein production

Designs for recombinant protein production were synthesized as individual gene fragments (Twist Biosciences). All constructs were codon-optimized for expression in Homo sapiens and cloned into pcDNA3.4 (Invitrogen) using Golden Gate cloning as described previously[6]. VHH-scFvs (functional assessment) were produced in a VHH-(G4S)3-scFv-6xHis format. VHH-Fcs (developability assessment) were produced in a VHH-G4S-Fc format. All in-house

produced Fc-tagged proteins are of human IgG1 antibody subclass and contain the L234A, L235A, P329G (LALA PG) mutations to reduce effector function[26].

For protein production of VHH-Fc and VHH-scFvs, plasmids were transiently transfected into ExpiCHO cells (1 µg DNA/mL) using the ExpiCHO Expression System (Gibco). Bispecific molecules were produced by co-transfecting three plasmids (the two heavy chains and the light chain) at a 1:1:1 ratio totaling 2 µg DNA/mL cell culture; chain-pairing mutations introduced between the two heavy chains enabled >90% correct heterodimer pairing directly from the production culture. Following harvest 6 days after transfection, the cell culture supernatant was clarified by centrifugation at 2000–3000 x g for 20–30 minutes. Concentrated (10x) phosphate-buffered saline (PBS), pH 7.4, was added to the supernatant to achieve a final concentration of 1x PBS.

Quantification of antibody titers

Antibody titer was quantified using BLI. The clarified supernatant was diluted 5-fold in Octet Buffer (composed of 1X PBS, 0.1% BSA, and 0.05% TWEEN20). Octet ProteinA biosensors (Sartorius) were hydrated in supernatant from an empty vector transfection 5-fold diluted in Octet buffer and equilibrated alongside the sample plate at 30°C for 10 minutes prior to the start of the experiment. Biosensors were shaken at 1000 rpm for 60 seconds in the samples. A standard curve was created using known concentrations of VHH-Fc diluted in mammalian supernatant and Octet buffer at a 1:4 dilution. Sample binding rate over the first 60 seconds of association to the biosensor was measured. Octet Analysis Studio 13.0.3.52 software was used to build the standard curve and apply it for quantitation of samples.

Protein purification

Recombinant proteins were purified from clarified ExpiCHO supernatant by batch affinity capture, with the capture chemistry selected according to the protein's affinity handle. Fc-containing proteins were purified using either rProtein A Sepharose Fast Flow antibody purification resin (Cytiva) or Mag Sepharose™ PrismA magnetic bead resin (Cytiva), and His-tagged proteins were purified using either Pierce™ High-Capacity EDTA-Compatible Ni-IMAC Resin or Pierce™ High-Capacity Ni-IMAC MagBeads, EDTA-compatible (Thermo Scientific).

For Fc-containing proteins, the resin/beads were equilibrated in 1x PBS, then added to the supernatant and mixed for 30 minutes to achieve binding. Two washes with 1x PBS were performed to remove residual supernatant and non-specific proteins, followed by two brief washes with water to remove residual PBS. Bound proteins were eluted with IgG Elution Buffer, pH 2.8 (Thermo Scientific), and immediately neutralized with 1 M Tris-HCl (Invitrogen) to approximately pH 7.

For His-tagged proteins, 10x nickel bind buffer (300 mM NaCl, 200 mM imidazole, 100 mM sodium phosphate, pH 8.0) was added to the clarified supernatant to a final 1x concentration. The resin/beads were equilibrated in a nickel bind buffer, then added to the conditioned supernatant and mixed for 30 minutes to achieve binding. The resin/beads were washed twice

with nickel wash buffer (300 mM NaCl, 40 mM imidazole, 20 mM sodium phosphate, pH 8.0), and bound proteins were eluted with elution buffer containing 500 mM imidazole. In both cases, the eluted protein was buffer exchanged into PBS using Zeba™ Spin Desalting Columns or Plates (Thermo Scientific), and the final protein concentration was quantified by A280.

NFAT-Luciferase Jurkat activation assay

For AFP, MAGE-A4, WT1, and NY-ESO-1 peptides, T2 cells (ATCC, CRL-1922) were harvested and resuspended in RPMI with 10% FBS at 1E6 cells/mL. Cells were pulsed with 50 µM peptide (Genscript, see Table 2) and 1 µg/mL β2 microglobulin (BD Biosciences) and incubated for 2 hours at 37°C. Following incubation, cells were aliquoted into a white flat-bottom, 96-well plate, 30k cells (30 µL) per well.

For KRAS peptides, HLA-A*03:01 A549 cells (BPS Bio, # 82469) were harvested the night prior to peptide pulsing and aliquoted into a white flat-bottom, 96-well plate, 20k cells per well in 100 µL of RPMI with 10% FBS. Cells were then allowed to adhere and grow overnight, incubated at 37°C. The next day, the supernatant was removed and the cells were pulsed with 50 µM peptide and 1 µg/mL β2 microglobulin in 30 µL of RPMI with 10% FBS per well. The cells were then incubated for 2 hours at 37°C.

Following peptide pulsing, NFAT Luciferase Reporter Jurkat cells (BPS Bio, # 60621) were harvested, resuspended at 0.5E6 cells/mL in RPMI with 10% FBS, and added to the 96-well assay plates, 30k cells (60 µL) per well. Bispecific T-cell engagers were prepared at 10 times the desired final concentration, arranged as either a single-point or titration. 10 µL of binder was then added to each well and gently mixed with a pipette. The assay was allowed to incubate at 37°C for 18 hours. The next day, a master mix of One-Step™ Luciferase Assay System (BPS Bio) was prepared, and 100 µL was added to each well. After a 15-min incubation at room temperature, the luminescence was measured on a Molecular Devices SpectraMax iD3 plate reader.

Table 2. MHC-I peptide reagent information

Name	**Sequence**	**Vendor (catalog #)**
AFP [158-166]	FMNKFIYEI	Genscript (RP30867-1)
MAGE-A4 [230-239]	GVYDGREHTV	Genscript (RP30866-1)
NY-ESO-1 [157-165]	SLLMWITQC	Genscript (RP30225)
WT1 [126-134]	RMFPNAPYL	Genscript (RP30863-1)
KRAS [7-16] G12V	VVVGAVGVGK	Genscript (RP30229)
NY-ESO-1 [157-165] C9V	SLLMWITQV	Genscript (RP21037)
NY-ESO-1 [157-165] S1A	ALLMWITQC	Genscript (custom synthesis)
NY-ESO-1 [157-165] L2A	SALMWITQC	Genscript (custom synthesis)

NY-ESO-1 [157-165] L3A	SLAMWITQC	Genscript (custom synthesis)
NY-ESO-1 [157-165] M4A	SLLAWITQC	Genscript (custom synthesis)
NY-ESO-1 [157-165] W5A	SLLMAITQC	Genscript (custom synthesis)
NY-ESO-1 [157-165] I6A	SLLMWATQC	Genscript (custom synthesis)
NY-ESO-1 [157-165] T7A	SLLMWIAQC	Genscript (custom synthesis)
NY-ESO-1 [157-165] Q8A	SLLMWITAC	Genscript (custom synthesis)
NY-ESO-1 [157-165] C9A	SLLMWITQA	Genscript (custom synthesis)
NY-ESO-1 [157-165] Off-Target 1	SLCQKIEQC	Genscript (custom synthesis)
NY-ESO-1 [157-165] Off-Target 2	SLLGGITVV	Genscript (custom synthesis)
NY-ESO-1 [157-165] Off-Target 3	SLLMSIHNI	Genscript (custom synthesis)
NY-ESO-1 [157-165] Off-Target 4	SLLNWRTKL	Genscript (custom synthesis)
NY-ESO-1 [157-165] Off-Target 5	TLLMVITGV	Genscript (custom synthesis)
KRAS [7-16]	VVVGAGGVGK	Genscript (RP30235)
KRAS [7-16] G12C	VVVGACGVGK	Genscript (RP30236)
KRAS [7-16] G12D	VVVGADGVGK	Genscript (RP30227)

PBMC cytotoxicity assay

Cryopreserved human PBMCs (BPS Bioscience) were thawed and rested overnight in RPMI-1640 supplemented with 10% FBS at 37 °C, 5% CO_2 prior to use. A549 cells engineered to express HLA-A*03:01 (BPS Bioscience*)* were used as targets. Target cells were labeled with CellTrace CFSE dye (Thermo Fisher) in PBS for 20 min at 37 °C, washed to quench excess dye, and seeded at 7,000 cells/well in 96-well flat-bottom plates. Cells were allowed to adhere overnight at 37 °C, 5% CO_2.

The following day, seeded target cells were pulsed with the corresponding KRAS-derived peptides shown in Table 2 (G12V, G12C, G12D, or wild-type) at a final concentration of 50 µM, or left unpulsed as a control. Recombinant human β2-microglobulin (BD Biosciences) was added concurrently at a final concentration of 1 µg/mL to stabilize surface peptide–MHC complexes. Cells were pulsed for 2h at 37 °C, 5% CO_2. Immediately following pulsing, rested PBMCs (effectors) were added together with serial antibody dilutions at an effector-to-target (E:T) ratio of 10:1. Co-cultures were incubated for 48 h at 37 °C, 5% CO_2. After incubation, culture supernatants were harvested and reserved. Adherent cells were detached by trypsinization, combined with the corresponding supernatant fraction to recover detached cells, and pelleted by centrifugation (250 x*g,* 5 min). Cells were resuspended and stained with 7-AAD (Thermo Fisher) for 15 min at 4 °C to discriminate viable from non-viable cells.

Samples were acquired on a NovoCyte Quanteon flow cytometer (Agilent). Target cells were identified as the $CFSE^+$ population, and target-cell viability was assessed by 7-AAD exclusion within this gate. Specific cytotoxicity was calculated relative to the antibody-free co-culture baseline for each condition as:

$$\% \text{ specific cytotoxicity} = (1 - (\% \text{ live\_TCE} / \% \text{ live\_no-TCE})) \times 100$$

where % live_TCE is the percentage of viable (7-AAD) cells within the $CFSE^+$ target gate, and %live_no-TCE is the corresponding value from the matched PBMC + target co-culture without antibody. Data were collected from 2 replicates; dose–response curves and EC50 values were determined by non-linear regression analysis in GraphPad Prism v11.

Cryo-EM sample preparation

For cryo-EM sample preparation, the *de novo* VHH-Fc construct was produced in ExpiCHO cells as described above, captured by Protein A affinity chromatography, and polished by size-exclusion chromatography (SEC) on a Superdex 200 column in 1× PBS. Biotinylated Human HLA-A*03:01&B2M&KRAS G12V (VVVGAVGVGK) Monomer Protein (MHC-HM418B) was purchased from KACTUS Biosciences and reconstituted to 3 mg/mL. An anti-β2-microglobulin Fab was included as a fiducial marker to add rigid mass to the complex and aid particle alignment during cryo-EM[27]. The Fab was generated by immobilized-ficin digestion of an azide-free, purified anti-human β2-microglobulin IgG1 monoclonal antibody (clone 2M2; BioLegend, 316302) using the Pierce Mouse IgG1 Fab and $F(ab')_2$ Preparation Kit (Thermo Fisher Scientific) and further purified by SEC. The SEC-purified Fab was concentrated to 4.5 mg/mL.

To assemble the complex, 326.69 µg of SEC-purified VHH-Fc was combined with 471 µg pMHC and 544.55 µg Fab — a 2.6 molar excess of both pMHC and Fab relative to the VHH-Fc — and incubated on ice for 30 minutes. The assembled complex was resolved from free pMHC and Fab by SEC on a Superdex 200 column in 1x PBS, and the peak fractions were concentrated to 1 mg/mL using a 10-kDa molecular-weight-cutoff Amicon Ultra centrifugal filter (2,000 x g).

Cryo-EM grid preparation and data acquisition

3 µL of pMHC-Fab-VHH-Fc complex was applied to 300-mesh UltrAuFoil R 1.2/1.3 grids that had been glow discharged (PELCO easiGlow™). Excess sample was blotted and grids were plunge-frozen in liquid ethane using Vitrobot Mark IV (Thermo Fisher Scientific). Micrographs were acquired using a Glacios transmission electron microscope (Thermo Fisher Scientific) operated at 200 kV and equipped with a Falcon 4 camera (Thermo Fisher Scientific). A total of 12,358 high magnification images were collected using Leginon software (Suloway et al., 2005) at 150,000x magnification with a calibrated pixel size of 0.93 Å/pixel and a dose rate of 6.98 $e^-/Å^2/s$ with a total exposure of 3.60 s, for an accumulated dose of 25.14 $e^-/Å^2$. Data were collected at a nominal defocus range of −1.0 to −2.5 µm.

Cryo-EM data processing

All data processing was carried out in cryoSPARC 4.7[28]. Images were preprocessed on-the-fly with CryoSPARC Live 4.7, and 11,028 micrographs were selected based on a CTF fit cutoff of 6 Å. 10 million particles were picked using a template picker and extracted. The extracted particles were subjected to three rounds of 2D classification and the best particles representing the intact complex were used to generate five ab initio models. Several iterative rounds of heterogeneous refinement, 3D classification, non-uniform refinement and CTF refinement were performed to select the homogenous conformation for final reconstruction. The final 3D reconstruction was generated using 566k particles and has a nominal resolution of 3.30 Å. To improve the resolution at the VHH-pMHC binding interface, local refinement was performed to obtain a 3.25 Å map of the region including the VHH and pMHC.

Cryo-EM model building

The $KRAS^{G12V}$-HLA structure (PDB 7STF[29]) and VHH (PDB 1I3V[30]) were docked into the cryo-EM map and used as an initial template for model building. Iterative rounds of manual adjustment in COOT[31] and real-space refinement in Phenix[32] were performed against the cryo-EM map to improve the stereochemistry as well as the model map coefficient correlation. Model validation of the final model was performed using MolProbity[33] in Phenix. An atomic model of the clone 2M2 Fab fragment could not be built due to the absence of sequence information from the supplier.

Monomericity - Size Exclusion Chromatography (SEC)

Proteins were analyzed using an Agilent 1100 system equipped with an AdvanceBio SEC 300Å column (PL1180-3301; Agilent), following a one-step Protein A purification. Affinity-purified samples were desalted into 1x PBS (pH 7.4) and diluted to 0.25 mg/mL. 6.25 µg of protein was injected using an autosampler and eluted at 1 mL/min using 150 mM sodium phosphate and 20 mM imidazole (pH 7.0) as the mobile phase. Chromatograms were analyzed with ChemStation software to determine percent monomer content.

Polyspecificity - PAIA ovalbumin assay

Ovalbumin binding was measured using PAIA Biotech developability kits (PA-DEV-OVA; PAIA Biotech). Samples were diluted to 67 nM in deionized water. 40 µL of PAIA reagent and 20 µL of sample were dispensed in duplicate into each well of the 384-well PAIA plate. Plates were shaken at 2200 rpm for 30 min, followed by 1500 rpm for 10 min, centrifuged briefly at 1500 x g, and read in bottom read mode at 630/670 nm. Data is presented as the average of two replicate wells. For PAIA assays, the results were normalized from 0 to 1, where 0 is the value associated with a low scoring control antibody (Trastuzumab) and 1 is the value associated with a high scoring control antibody (Bococizumab).

Polyspecificity - Baculovirus Particle (BVP) ELISA

25 µL of 1% baculovirus particles in PBS (MEDNA Scientific) were diluted with equal volume of 50 mM sodium carbonate (pH 9.6) per well, and incubated on high bind ELISA plates (3925;

Corning) at 4°C overnight with shaking. The next day, unbound BVPs were removed from the wells and the plate was washed 3x with 100 µL of 1x PBS. All remaining steps were performed at room temperature. 100 µL of blocking buffer (PBS with 0.5% BSA) was added to the plate and incubated for 1 hour with shaking at 450 rpm. Following incubation, the plate was washed 3x with 100 µL of 1x PBS. Next, antibodies were diluted to 100 nM in blocking buffer and wells were treated with 50 µL for 1 hour with shaking at 450 rpm. The plate was then washed 6x with 100 µL of 1x PBS. 50 µL of 100 ng/mL secondary anti-Fc-HRP conjugate (Thermo A18817) was added to the wells and incubated for 1 hour. The plate was then washed 6x with 100 µL of 1x PBS. Finally, 100 µL of room temperature QuantaBlu Working Solution (Thermo, 15169), a 9:1 mixture of QuantaBlu Substrate Solution and QuantaBlu Stable Peroxide Solution, was added to each well and incubated for 5 minutes with shaking at 450 rpm. The reactions were stopped by addition of 100 µL QuantaBlu Stop Solution to each well. Endpoint fluorescence with excitation at 325 nm and emission at 420 nm was read on an iD3 SpectraMax Microplate Reader (Molecular Devices). BVP scores were determined by normalizing raw fluorescence values to control wells with no test antibody (i.e. BVP-only control). Data is presented as the average of two replicate wells. The results were normalized from 0 to 1, where 0 is the value associated with a low BVP binding control antibody (Trastuzumab) and 1 is the value associated with a high BVP binding control antibody (Bococizumab).

Differential scanning fluorimetry (DSF)

Thermal stability was assessed by differential scanning fluorimetry using the GloMelt™ Thermal Shift Protein Stability Kit (Biotium, cat. no. 33021) according to the manufacturer's protocol. Briefly, The 200X GloMelt™ dye stock was diluted to 10X in PBS, and 2 µL of the 10X dye was added to 18 µL of protein at 0.5 mg/mL (9 µg total protein) for a final reaction volume of 20 µL containing 1X dye. Reactions were assembled in a 96-well qPCR plate, sealed, and briefly centrifuged. Fluorescence was monitored in the FAM channel on a Biorad CFX opus qPCR while the temperature was ramped from 25 °C to 95 °C at 2.4 °C/min. The melting temperature (Tm) was determined from the first derivative of the fluorescence versus temperature curve, taken as the temperature of the first resolved melting transition.

On-cell affinity - Flow cytometry

HLA-A*03:01 A549 cells were harvested and resuspended in RPMI with 10% FBS at 1E6 cells/mL and 1 µg/mL β2 microglobulin. Cells were pulsed with 50 µM peptide or left unpulsed and incubated for 2 hours at 37°C. Following the peptide pulse, cells were pipetted to a v-bottom 96-well plate at 0.1E6 cells/well and washed twice with cold PBSA. Antibody serial dilutions were prepared manually and added to the cells. The primary stain was then allowed to incubate for 2 hours at 4°C. The cells were washed four times with cold PBSA, after which a secondary antibody was added and incubated for 30 minutes at 4°C. For VHH-Fc format, the cells were stained with anti-Human_Fc-AF647 antibody (Biolegend), and for VHH-scFv format the cells were stained with anti-His-AF647 antibody (R&D Systems). The cells were then washed twice with cold PBSA. Lastly, the fluorescence was measured on a Novocyte Advanteon flow cytometer (Agilent).

Recombinant affinity - Biolayer Interferometry (BLI)

An RH96 Octet system with 384-Well Tilted-Bottom Microplates (Sartorius) was used to determine binding kinetics of designs in VHH-scFv format to immobilized pMHC monomer. Briefly, Octet SAX2 biosensors (Sartorius) were hydrated in an Octet buffer composed of 1x PBS, 0.1% BSA, and 0.05% TWEEN20, and equilibrated alongside the sample plate at 30°C for 10 minutes prior to start of the experiment. Octet SAX2 biosensors (Sartorius) were equilibrated in the Octet buffer for 60 seconds prior to loading with 50 nM biotinylated KRAS G12V pMHC monomer (KACTUS Bio, MHC-HM418B) in Octet buffer to a target loading density of 0.20 nm.

The biosensors were then baselined in the Octet buffer for 60 seconds before initiating the association phase. During this phase, the biosensors were exposed to multiple VHH-scFv concentrations ranging from 7.8 nM to 500 nM in Octet buffer for 300 seconds. Following the association phase, a 300-second dissociation phase in the Octet buffer was assessed. A reference sample containing only the Octet buffer was included and used for data correction.

A 1:1 model global fit of the association and dissociation was used to determine K_D in the Octet Analysis Studio 13.0.3.52 software.

Acknowledgements

Cryo-EM data collection, data processing, and model building were performed by NanoImaging Services, Inc.

References

1. Thul, P. J. et al. A subcellular map of the human proteome. Science 356, eaal3321 (2017).
2. Neefjes, J., Jongsma, M. L. M., Paul, P. & Bakke, O. Towards a systems understanding of MHC class I and MHC class II antigen presentation. Nature Reviews Immunology 11, 823–836 (2011).
3. Hsiue, E. H.-C. et al. Targeting a neoantigen derived from a common TP53 mutation. Science 371, eabc8697 (2021).
4. Douglass, J. et al. Bispecific antibodies targeting mutant RAS neoantigens. Science Immunology 6, eabd5515 (2021).
5. Nathan, P. et al. Overall survival benefit with tebentafusp in metastatic uveal melanoma. New England Journal of Medicine 385, 1196–1206 (2021).
6. Nabla Bio. JAM-2: de novo design of drug-like antibodies. https://nabla-public.s3.us-east-1.amazonaws.com/2025_Nabla_JAM2.pdf (2025).
7. Liu, B. et al. Design of high-specificity binders for peptide–MHC-I complexes. Science 389, 386–391 (2025).
8. Johansen, K. H. et al. De novo-designed pMHC binders facilitate T cell–mediated cytotoxicity toward cancer cells. Science 389, 380–385 (2025).
9. Householder, K. D. et al. De novo design and structure of a peptide-centric TCR mimic binding module. Science 389, 375–379 (2025).
10. Bennett, N. R. et al. Atomically accurate de novo design of antibodies with RFdiffusion. Nature 649, 183–193 (2025).
11. Chai Discovery. Drug-like antibody design against challenging targets with atomic precision. Preprint at https://doi.org/10.1101/2025.11.29.691346 (2025).
12. Prior, I. A., Hood, F. E. & Hartley, J. L. The frequency of Ras mutations in cancer. Cancer Research 80, 2969–2974 (2020).
13. Cox, A. D., Fesik, S. W., Kimmelman, A. C., Luo, J. & Der, C. J. Drugging the undruggable RAS: mission possible? Nature Reviews Drug Discovery 13, 828–851 (2014).
14. Liu, L. et al. MGD011, a CD19 × CD3 dual-affinity retargeting bi-specific molecule incorporating extended circulating half-life for the treatment of B-cell malignancies. Clinical Cancer Research 23, 1506–1518 (2017).
15. Shiku, H. et al. Bispecific antibody. US patent US20230287121A1 (2023).
16. Stewart-Jones, G. et al. Rational development of high-affinity T-cell receptor-like antibodies. Proceedings of the National Academy of Sciences 106, 5784–5788 (2009).
17. Chen, J.-L. et al. Identification of NY-ESO-1 peptide analogues capable of improved stimulation of tumor-reactive CTL. The Journal of Immunology 165, 948–955 (2000).
18. Chen, J.-L. et al. Structural and kinetic basis for heightened immunogenicity of T cell vaccines. Journal of Experimental Medicine 201, 1243–1255 (2005).
19. Du, J., Tang, W., Zhao, L., Jiao, X. & Du, P. Anti-KRAS/HLA antibodies and uses thereof. International patent WO2024230588A1 (2024).

20. Kontermann, R. E. & Brinkmann, U. Bispecific antibodies. Drug Discovery Today 20, 838–847 (2015).
21. Labrijn, A. F., Janmaat, M. L., Reichert, J. M. & Parren, P. W. H. I. Bispecific antibodies: a mechanistic review of the pipeline. Nature Reviews Drug Discovery 18, 585–608 (2019).
22. Ridgway, J. B., Presta, L. G. & Carter, P. 'Knobs-into-holes' engineering of antibody CH3 domains for heavy chain heterodimerization. Protein Engineering 9, 617–621 (1996).
23. Biswas, S. et al. De novo design of epitope-specific antibodies against soluble and multipass membrane proteins with high specificity, developability, and function. Preprint at https://doi.org/10.1101/2025.01.21.633066 (2025).
24. Jain, T. et al. Biophysical properties of the clinical-stage antibody landscape. Proceedings of the National Academy of Sciences 114, 944–949 (2017).
25. Van Deventer, J. A. & Wittrup, K. D. Yeast surface display for antibody isolation: library construction, library screening, and affinity maturation. Methods in Molecular Biology 1131, 151–181 (2014).
26. Schlothauer, T. et al. Novel human IgG1 and IgG4 Fc-engineered antibodies with completely abolished immune effector functions. Protein Engineering, Design and Selection 29, 457–466 (2016).
27. Saotome, K. et al. Structural analysis of cancer-relevant TCR–CD3 and peptide–MHC complexes by cryo-EM. Nature Communications 14, 2401 (2023).
28. Punjani, A., Rubinstein, J. L., Fleet, D. J. & Brubaker, M. A. cryoSPARC: algorithms for rapid unsupervised cryo-EM structure determination. Nature Methods 14, 290–296 (2017).
29. Wright, K. M. et al. Hydrophobic interactions dominate the recognition of a KRAS G12V neoantigen. Nature Communications 14, 5063 (2023).
30. Spinelli, S., Tegoni, M., Frenken, L., van Vliet, C. & Cambillau, C. Lateral recognition of a dye hapten by a llama VHH domain. Journal of Molecular Biology 311, 123–129 (2001).
31. Emsley, P., Lohkamp, B., Scott, W. G. & Cowtan, K. Features and development of Coot. Acta Crystallographica Section D: Biological Crystallography 66, 486–501 (2010).
32. Adams, P. D. et al. PHENIX: a comprehensive Python-based system for macromolecular structure solution. Acta Crystallographica Section D: Biological Crystallography 66, 213–221 (2010).
33. Davis, I. W., Murray, L. W., Richardson, J. S. & Richardson, D. C. MolProbity: structure validation and all-atom contact analysis for nucleic acids and their complexes. Nucleic Acids Research 32, W615–W619 (2004).

Supplemental Information

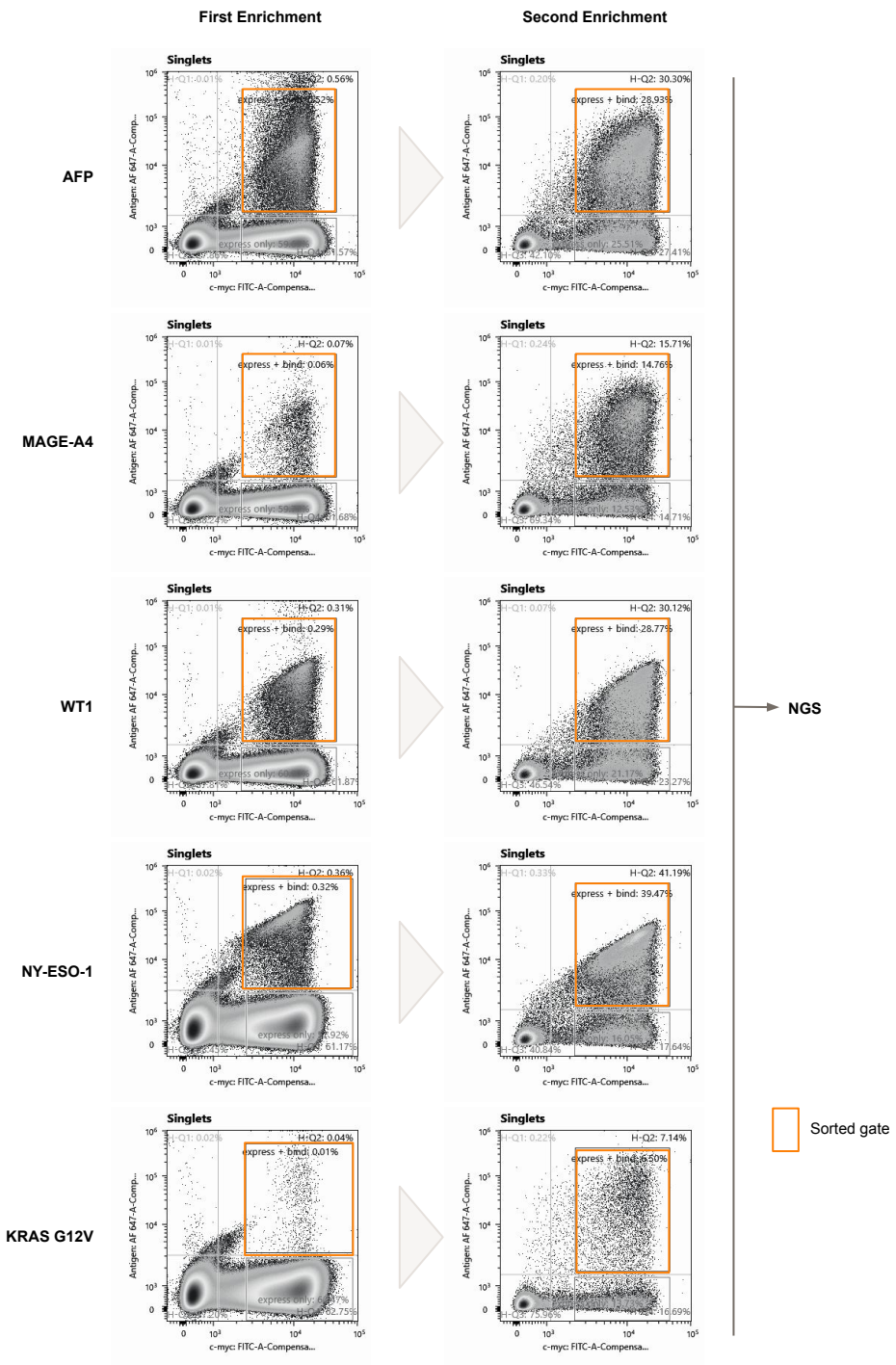

Supplementary Figure 1. Two rounds of FACS enrichment isolate target-binding *de novo* designs across five pMHC antigens. FACS plots of yeast surface displayed designs showing initial enrichments at 10 nM antigen for AFP, MAGE-A4, WT1 and NY-ESO-1 and 100 nM for KRAS G12V. A second enrichment was then performed at the same concentration of antigen. These doubly enriched populations were then sequenced by NGS.

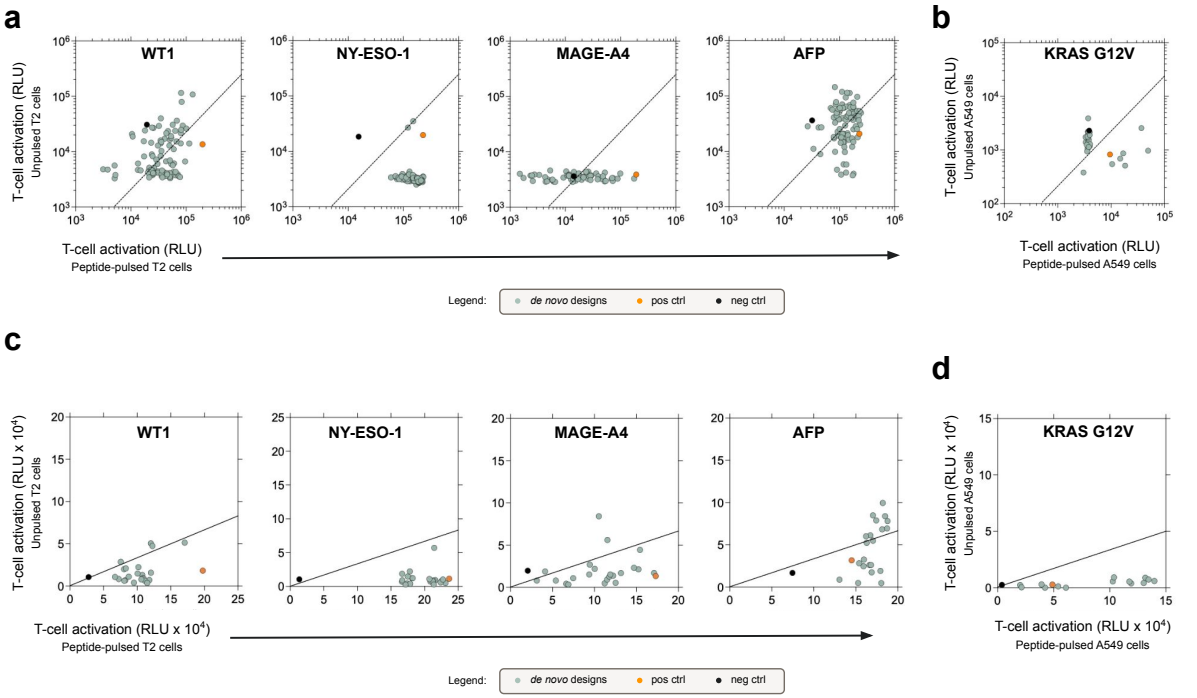

Supplementary Figure 2: JAM-2 generated *de novo* designs produce peptide-specific T-cell activation. Jurkat NFAT-luciferase reporter activation against *de novo* designs, measured in coculture with cells pulsed with the indicated peptide (x-axis) versus unpulsed cells (y-axis); the dashed line marks a 3-fold threshold. **(a,b)** single-concentration screen at 10 nM for **(a)** WT1, NY-ESO-1, MAGE-A4, and AFP on T2 (HLA-A*02:01) cells and **(b)** KRAS G12V on A549–HLA-A*03:01 cells. **(c,d)** For 16-24 selected designs per target, titrations (up to 250 nM) were performed to calculate EC50s, with reporter activation at the top dose shown for **(c)** WT1, NY-ESO-1, MAGE-A4, and AFP on T2 (HLA-A*02:01) cells and **(d)** KRAS G12V on A549–HLA-A*03:01 cells. For each target, a positive control (orange) was included, each of which was discovered via phage display against the pMHC antigen: HLA-A*02:01/WT1 (Hoffmann-La Roche)[1], anti-HLA-A*02:01/NY-ESO-1 (Daiichi Sankyo)[2], HLA-A*02:01/MAGE-A4 (Hoffmann-La Roche)[3], HLA-A*02:01/AFP (Eureka Therapeutics)[4], and HLA-A*03:01/KRAS G12V (Biocytogen)[5]. All panels include a negative isotype control (black): a JAM-2 *de novo*-designed VHH directed against an unrelated target, which controls for non-specific reporter activation from the design format. Pulsed targets gave strong reporter signal while unpulsed targets generally remained near background, indicating peptide-dependent activation.

References

1. Benz, J. et al. Antibodies binding to HLA-A2/WT1. U.S. Patent US20190248916A1 (2019).
2. Shiku, H. et al. Bispecific antibody. U.S. Patent US20230287121A1 (2023).
3. Weinzierl, T. et al. Antibodies binding to HLA-A2/MAGE-A4. World Patent WO2021122875A1 (2021).
4. Liu, C., Liu, H., Xu, Y., Xiang, J. & Long, L. Constructs targeting AFP peptide/MHC complexes and uses thereof. U.S. Patent US10011658B2 (2018).
5. Du, J., Tang, W., Zhao, L., Jiao, X. & Du, P. Anti-KRAS/HLA antibodies and uses thereof. World Patent WO2024230588A1 (2024).

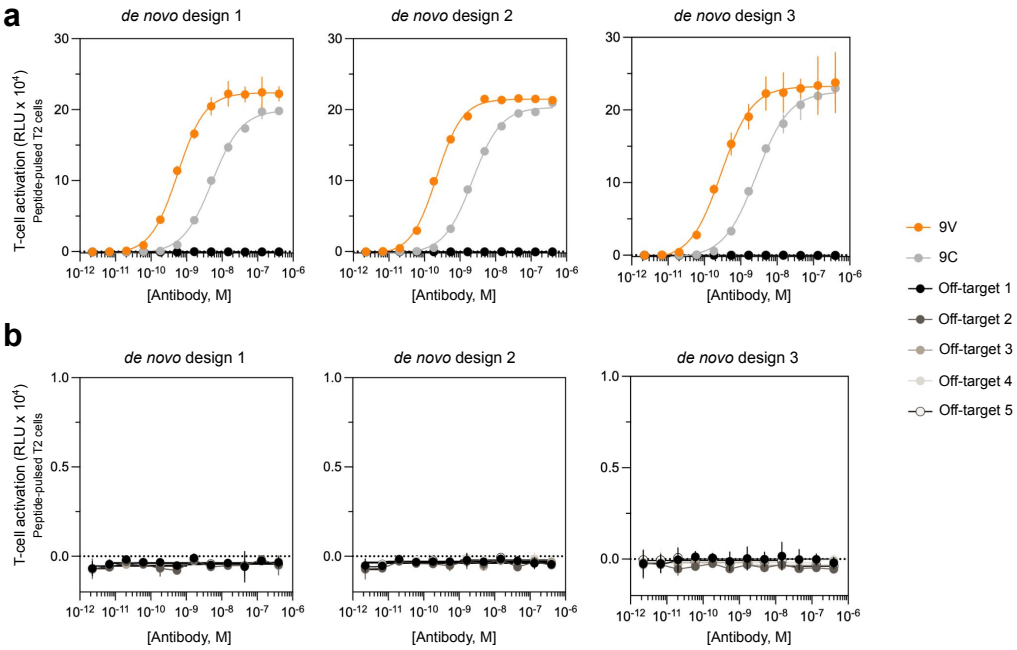

Supplementary Figure 3: JAM-2-generated *de novo* designs yields dose-dependent, on-target T-cell activation with no off-target response. Jurkat NFAT-luciferase reporter activation across a titration of three JAM-2-generated *de novo* antibody designs (columns). Each design was titrated against T2 cells pulsed with the two NY-ESO-1 on-target peptides (9V, 9C) and five off-target peptides (Off-target 1–5). **(a)** For all three designs, both on-target peptides drove dose-dependent activation, while the off-target peptides remained flat at background. **(b)** The same data as for off-target peptides only with the y-axis expanded ~30-fold (≤1 × 10^4 RLU) to resolve the off-target traces; none of the five off-target peptides produced dose-dependent activation, staying at or near background (dotted line at zero) across the full concentration range. Points represent mean ± s.d. of 2 replicates.

Name	Peptide	IC50 (nM)	Percentile rank	IC50 relative to wild-type	Percentile rank relative to wild-type
Wild-type	SLLMWITQC	422.15	2.1	1.000	1.000
S1A	ALLMWITQC	736.18	2.8	1.744	1.333
L2A	SALMWITQC	10449.59	15	24.753	7.143
L3A	SLAMWITQC	452.58	2.2	1.072	1.048
M4A	SLLAWITQC	102.1	0.76	0.242	0.362
W5A	SLLMAITQC	1059.93	3.3	2.511	1.571
I6A	SLLMWATQC	1361.57	3.8	3.225	1.810
T7A	SLLMWIAQC	390.92	2	0.926	0.952
Q8A	SLLMWITAC	483.55	2.2	1.145	1.048
C9A	SLLMWITQA	17.12	0.16	0.041	0.076
C9V	SLLMWITQV	4.55	0.03	0.011	0.014

Supplementary Table 1: Alanine substitutions across the NY-ESO-1 peptide largely preserve predicted HLA-A*02:01 binding affinity. NetMHCpan 4.1[1] BA binding predictions (IC50) and percentile ranks for HLA-A*02:01 MHC-I for the wild-type NY-ESO-1 peptide, its corresponding alanine-scanning variants, and the anchor modified C9V analog. To facilitate direct comparison against wild-type baselines, raw IC50 values and percentile ranks were normalized by dividing each variant metric by its respective wild-type value. Relative values near 1.0 indicate preserved predicted binding, while elevated relative values signify a predicted reduction in HLA-A*02:01 stabilization, confirming that central residue modifications do not disrupt complex presentation.

References

1. Reynisson, B., Alvarez, B., Paul, S., Peters, B. & Nielsen, M. NetMHCpan-4.1 and NetMHCIIpan-4.0: improved predictions of MHC antigen presentation by concurrent motif deconvolution and integration of MS MHC eluted ligand data. Nucleic Acids Research 48, W449–W454 (2020)

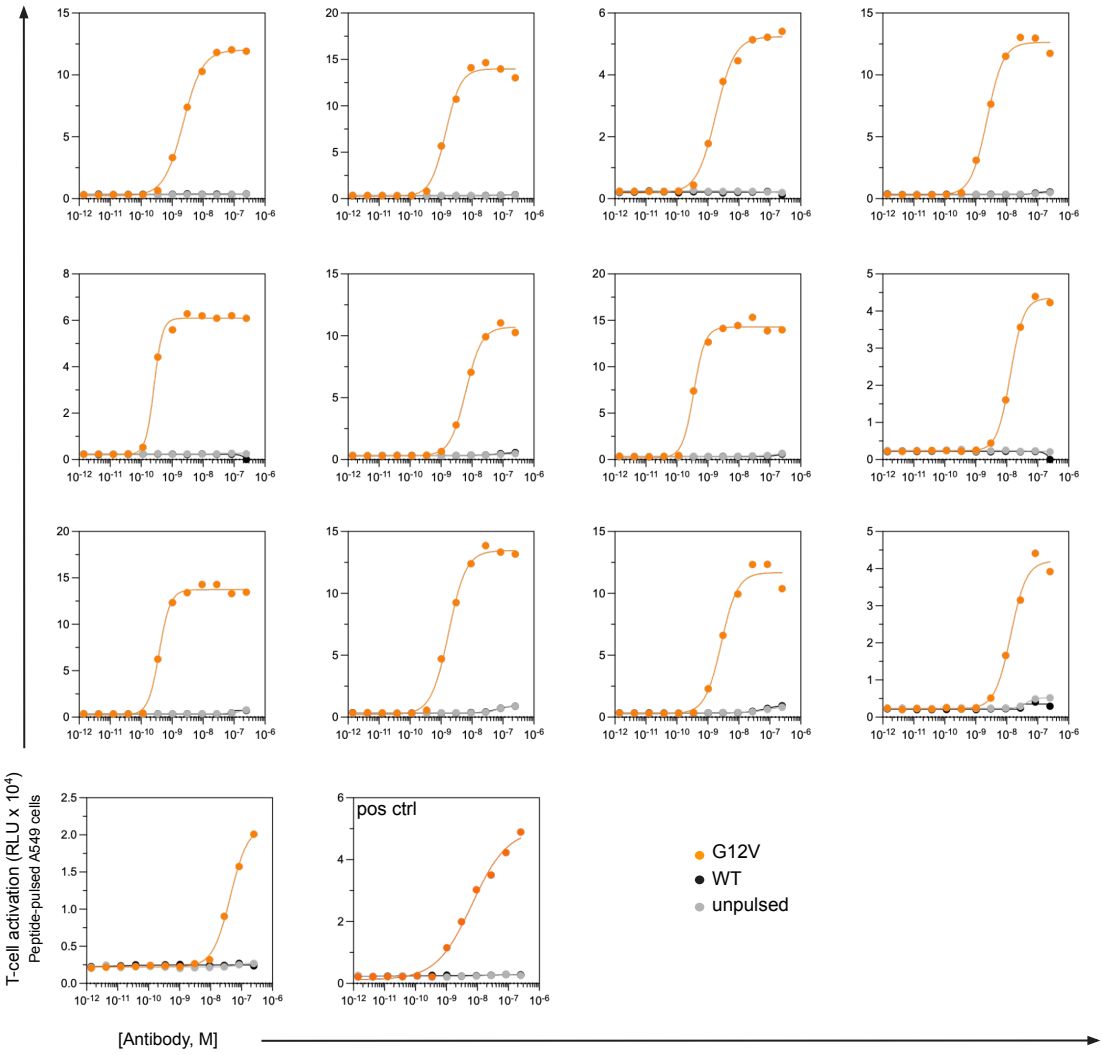

Supplementary Figure 4: *De novo* designs against KRAS G12V are mutation-selective. Jurkat NFAT-luciferase reporter activation in peptide-pulsed A549–HLA-A*03:01 cells across a titration of 13 JAM-2-generated *de novo* antibody designs targeting the KRAS G12V neoepitope and the positive control (phage-display-derived KRAS G12V-targeting antibody from Biocytogen[1]). Each design was tested against the mutant peptide (G12V, orange), the wild-type KRAS peptide (WT, black), and unpulsed cells (grey). Designs gave dose-dependent activation against G12V while remaining at or within 3X of background against both the WT peptide and unpulsed controls, indicating mutation-selective recognition. Points represent single measurements.

References:

1. Du, J., Tang, W., Zhao, L., Jiao, X. & Du, P. Anti-KRAS/HLA antibodies and uses thereof. World Patent WO2024230588A1 (2024).

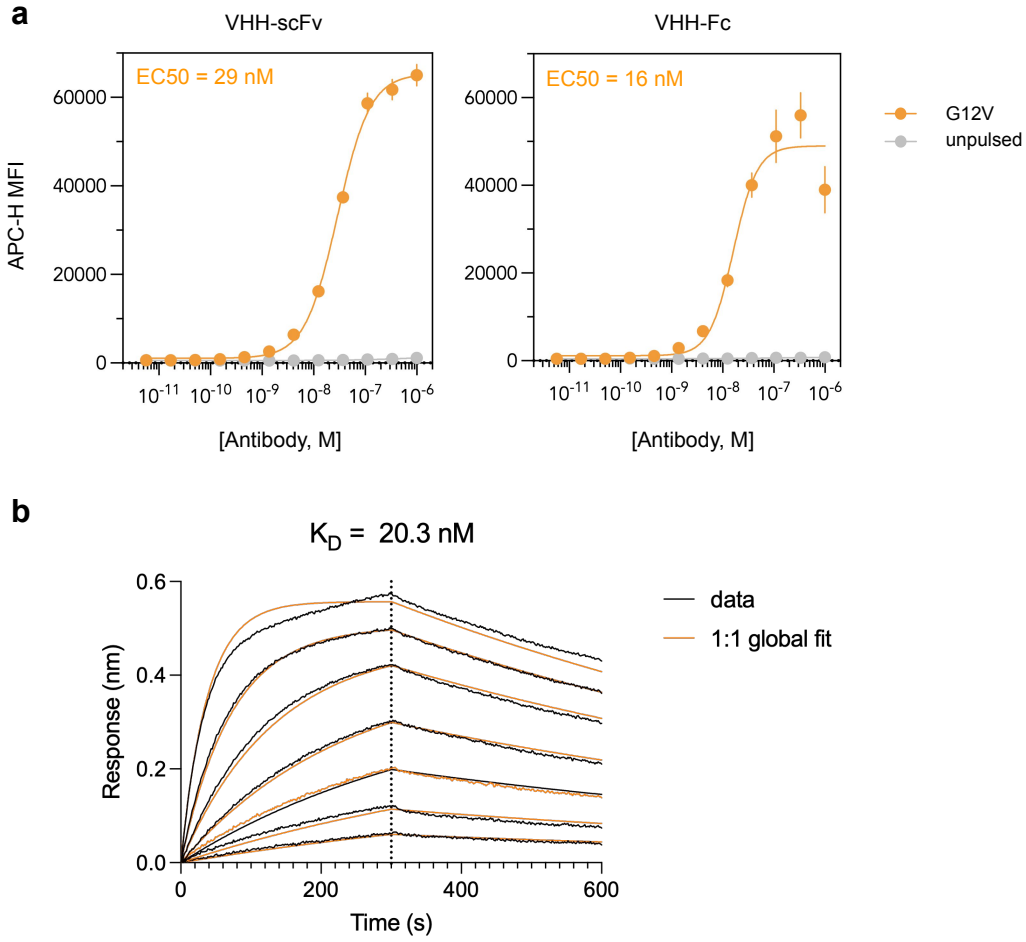

Supplementary Figure 5: Dual-variant binding anti-KRAS G12V design submitted for cryo-EM shows low double digit nM K_D by flow cytometry and BLI. (a) Antibody titrations measured via flow cytometry for the lead anti-KRAS G12V design in two formats: VHH-Fc and VHH-scFv. HLA-A*03:01$^+$ A549 cells were pulsed with the KRAS G12V peptide or left unpulsed, then stained with a serial dilution of antibody. The EC50 value derived from the curve fit is reported in each plot. Points represent mean ± s.d. of 2 replicates. **(b)** BLI sensorgrams showing binding in VHH-scFv format to immobilized biotinylated KRAS G12V pMHC monomer (KACTUS Bio, MHC-HM418B). Binding was assessed at concentrations of VHH-scFv ranging from 7.8 nM to 500 nM. A K_D of 20.3 nM was obtained from 1:1 global fit.

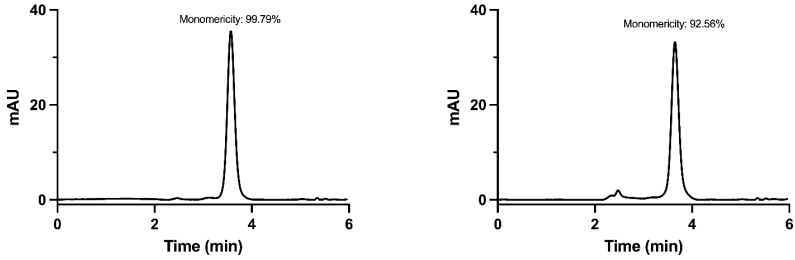

Supplementary Figure 6: Analytical SEC validation shows >90% monomericity of *de novo* VHH designs reformatted into asymmetric IgG-like bispecific antibodies. Size-exclusion chromatograms of two KRAS-targeting VHH candidates reformatted as knobs-into-holes (KiH) heterodimers with an anti-CD3ε Fab arm (derived from Duvortuxizumab[1]). Each construct eluted as a single dominant peak at a retention volume consistent with the correctly assembled heterodimer.

References

1. Liu, L. et al. MGD011, a CD19 × CD3 dual-affinity retargeting bi-specific molecule incorporating extended circulating half-life for the treatment of B-cell malignancies. Clinical Cancer Research 23, 1506–1518 (2017)

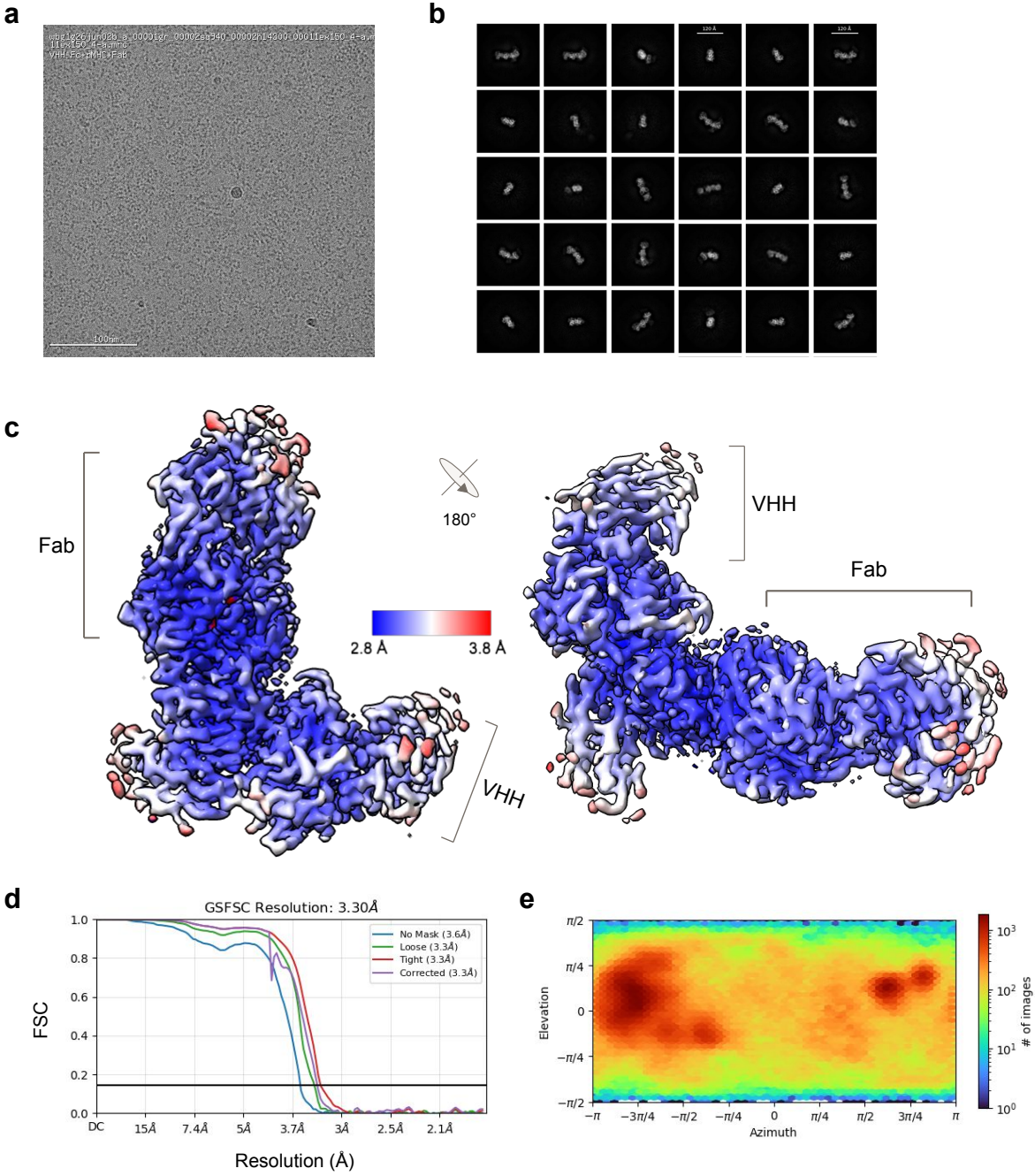

Supplementary Figure 7. Single-particle cryo-EM reconstruction resolves the binding interface of a *de novo* VHH with KRAS G12V pMHC monomer. (**a**) Representative micrograph illustrating particle distribution and contrast. Scale Bar: 100 nm. (**b**) 2D class averages of VHH-pMHC-Fab complex shown for a range of particle angles (**c**) Electron density map with local resolution (full map) calculated using an FSC value of 0.143 (**d**) Fourier Shell Correlation (FSC) plot (full map) where the FSC curve is plotted against spatial frequency, with the x-axis labeled in real-space resolution (Å) for clarity (**e**) Viewing direction distribution plot showing the angular assignment of particles contributing to the final map.

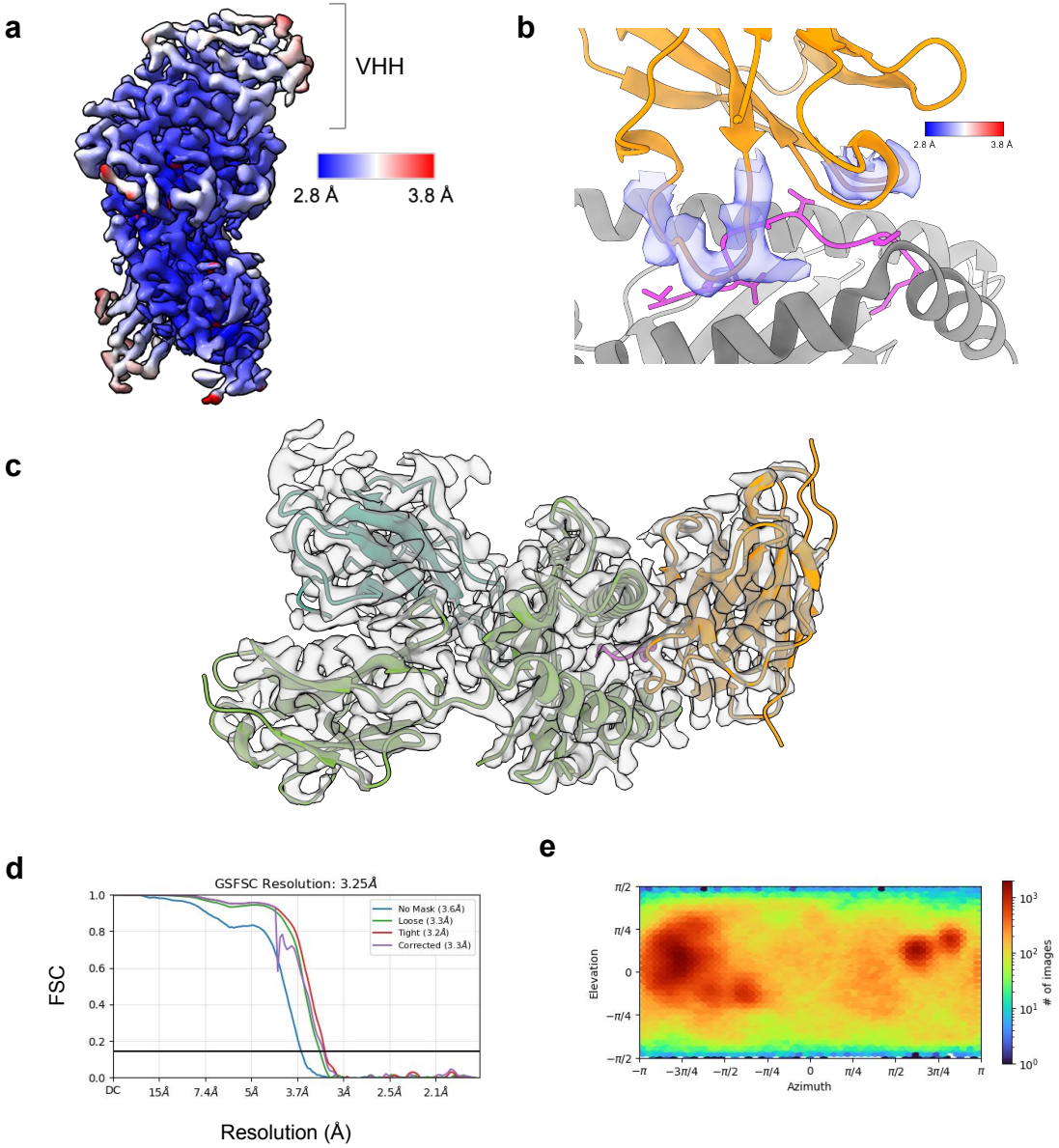

Supplementary Figure 8: Local refinement improves map resolution at the *de novo* VHH–pMHC interface. Local masking and refinement were performed to mitigate conformational flexibility from the anti-β2m Fab arm. (**a**) Electron density map with local resolution following focused refinement (FSC = 0.143) (**b**) Cutaway view of electron density map showing sub-3 Å local resolution at interface residues. (**c**) Electron density map overlaid on fit PDB model (VHH, orange; KRAS G12V peptide, magenta; MHC, light green; β2m, light blue). (**d**) Focused map FSC plot for local refinement map with spatial frequency mapped to real-space resolution (Å) (**e**) Viewing direction distribution plot showing the angular assignment of particles contributing to the locally refined reconstruction.

Data collection and processing	
Microscope	Glacios (Thermo Fisher)
Voltage (kV)	200
Detector, mode	Falcon 4, counting
Automation software	Leginon
Nominal magnification	150,000x
Pixel size (Å)	0.93
Defocus range (μm)	−1.0 to −2.5
Dose rate (e^-/Å²/s)	6.98
Exposure time (s)	3.6
Total dose (e^-/Å²)	25.14
Micrographs collected / used	12,358 / 11,028
Symmetry imposed	C1
Particles extracted	~10,000,000
Particles in final map	566,000
Map resolution, consensus (FSC 0.143) (Å)	3.3
Map resolution, local refinement (FSC 0.143) (Å)	3.25
Refinement	
Initial models (PDB)	7STF, 1I3V
Model resolution, FSC 0.5 (Å)	3.4
Map sharpening B factor (Å²) consensus / local	150.6 / 146.3
Non-H atoms / protein residues / ligands	4,069 / 509 / 0
B-factors, protein min/max/mean (Å²)	0.00 / 134.25 / 49.17
RMSD bonds (Å) / angles (°)	0.005 / 0.670
Validation	
MolProbity score	2.01
Clashscore	12.59
Rotamer outliers (%)	0.69
Ramachandran favored/allowed/outliers (%)	94.01 / 5.99 / 0.00
Cβ outliers (%)	0.00
CaBLAM outliers (%)	2.43
Map-model CC (mask / volume)	0.81 / 0.77

Supplementary Table 2: Cryo-EM data collection, refinement, and validation statistics. Refinement and validation statistics correspond to the locally refined map (VHH–pMHC); the anti-β2-microglobulin Fab fiducial aided alignment and was not modeled.

PDB References

1. **7STF:** Wright, K. M. et al. Hydrophobic interactions dominate the recognition of a KRAS G12V neoantigen. Nature Communications 14, 5063 (2023).
2. **1I3V:** Spinelli, S., Tegoni, M., Frenken, L., van Vliet, C. & Cambillau, C. Lateral recognition of a dye hapten by a llama VHH domain. Journal of Molecular Biology 311, 123–129 (2001).